Developmental Biology 363 (2012) 201–218

Contents lists available at SciVerse ScienceDirect

Developmental Biology

journal homepage: www.elsevier.com/developmentalbiology

STELLA-positive subregions of the primitive streak contribute to posterior tissues of the mouse gastrula

Maria M. Mikedis [1], Karen M. Downs *

Department of Cell and Regenerative Biology, University of Wisconsin-Madison School of Medicine and Public Health, 1300 University Ave, Madison, WI 53706, USA

ARTICLE INFO

Article history:
Received for publication 6 April 2011
Revised 26 August 2011
Accepted 2 October 2011
Available online 8 October 2011

Keywords:
Allantois
Allantoic Core Domain
Amnion
Blood islands
Chorionic ectoderm
Dorsal aortae
DPPA3
Hematopoietic cells
Hindgut
Mouse
Omphalomesenteric artery
Primitive streak
PGC7
Primordial germ cells
Somatopleure
Splanchnopleure
STELLA
Ventral ectodermal ridge
Yolk sac

ABSTRACT

The developmental relationship between the posterior embryonic and extraembryonic regions of the mammalian gastrula is poorly understood. Although many different cell types are deployed within this region, only the primordial germ cells (PGCs) have been closely studied. Recent evidence has suggested that the allantois, within which the PGCs temporarily take up residence, contains a pool of cells, called the Allantoic Core Domain (ACD), critical for allantoic elongation to the chorion. Here, we have asked whether the STELLA-positive cells found within this region, thought to be specified PGCs, are actually part of the ACD and to what extent they, and other ACD cells, contribute to the allantois and fetal tissues. To address these hypotheses, STELLA was immunolocalized to the mouse gastrula between Early Streak (ES) and 12-somite pair (-s) stages (~6.75–9.0 days post coitum, dpc) in histological sections. STELLA was found in both the nucleus and cytoplasm in a variety of cell types, both within and outside of the putative PGC trajectory. Fate-mapping the headfold-stage (~7.75–8.0 dpc) posterior region, by which time PGCs are thought to be segregated into a distinct lineage, revealed that the STELLA-positive proximal ACD and intraembryonic posterior primitive streak (IPS) contributed to a wide range of somatic tissues that encompassed derivatives of the three primary germ layers. This contribution included STELLA-positive cells localizing to tissues both within and outside of the putative PGC trajectory. Thus, while STELLA may identify a subpopulation of cells destined for the PGC lineage, our findings reveal that it may be part of a broader niche that encompasses the ACD and through which the STELLA population may contribute cells to a wide variety of posterior tissues of the mouse gastrula.

Introduction

A range of embryonic and extraembryonic tissues, including the amnion, allantois, blood vessels, hindgut, surface ectoderm, tailbud, and primordial germ cells (PGCs), are deployed and develop together in the posterior region of the mammalian conceptus. However, with the exception of the PGCs, the origin of these posterior cell types is still largely obscure.

PGCs are thought to originate from the proximal epiblast of the mouse conceptus at ~6.25–6.5 dpc (Lawson and Hage, 1994; Ohinata et al., 2005). Although the timing of PGC specification is controversial (Lawson and Hage, 1994; Ohinata et al., 2005), epiblast cells assumed to be destined for the gonads migrate through the primitive streak, and then reside temporarily within the base of the allantois/posterior embryonic region (Chiquoine, 1954; Ginsburg et al., 1990; Lawson and Hage, 1994; Ozdzenski, 1967; Saitou et al., 2002), where additional signals may induce PGC specification (Fujiwara et al., 2001). From the allantois/posterior embryonic region, the putative PGCs translocate into the hindgut endoderm (~8.5 dpc); between ~9.5 and 10.0 dpc, the PGCs exit the hindgut and migrate towards the developing genital ridges, which they colonize between ~10.0 and 11.5 dpc (reviewed in Molyneaux and Wylie, 2004). Within the gonads, PGCs complete their development as germ cells and form sperm and eggs.

Abbreviations: ACD, Allantoic Core Domain; AX, allantois-associated extraembryonic visceral endoderm; DCM, dorsal cuboidal mesothelium; dpc, days post coitum; EB, Early Bud; EHF, Early Headfold; ES, Early Streak; EVE, embryonic visceral endoderm; IPS, intraembryonic posterior primitive streak; LB, Late Bud; LHF, Late Headfold; OB, No Allantoic Bud; PBS, phosphate-buffered saline; PFA, paraformaldehyde; PGCs, primordial germ cells; s, somite pairs; T, Brachyury; TNAP, tissue-nonspecific alkaline phosphatase; vEHF, very Early Headfold; VCM, ventral cuboidal mesothelium; XVE, extraembryonic visceral endoderm; XPS, extraembryonic posterior primitive streak.

* Corresponding author. Fax: +1 608 262 7306.
E-mail address: kdowns@wisc.edu (K.M. Downs).
[1] Fax: +1 608 262 7306.

0012-1606/$ – see front matter © 2011 Elsevier Inc. All rights reserved.
doi:10.1016/j.ydbio.2011.10.003

The PGC trajectory was established using tissue non-specific alkaline phosphatase (TNAP) activity (Macgregor et al., 1995) as a "marker" for PGCs (Chiquoine, 1954; Ozdzenski, 1967; Tam and Snow, 1981) in conjunction with *Dominant white spotting* (*W*) and *Steel* (*Sl*) mutants (McCoshen and McCallion, 1975; Mintz, 1957; Mintz and Russell, 1957). In these sterile mutants, TNAP-positive cells formed in the posterior region of the conceptus in numbers similar to wildtype. During hindgut migration, the number of TNAP-positive cells became greatly reduced in the mutants, and then significantly reduced or absent in the early gonad. Yet, although TNAP is thought to mark PGCs, it is not required for successful PGC formation, migration, and colonization of the gonads (Macgregor et al., 1995).

Recently, other proteins have been reported to be associated with the emergence of the germ line, including BLIMP1 (PRDM1) and STELLA (DPPA3, PGC7). BLIMP1, a transcriptional repressor of the somatic program within putative PGCs (Kurimoto et al., 2008; Ohinata et al., 2005), is thought to be required for the formation of the nascent putative PGC population, as *Blimp1* null mutants exhibit fewer TNAP-positive cells in the posterior region as early as ~7.5–7.75 dpc (Ohinata et al., 2005; Vincent et al., 2005). STELLA, a maternally inherited factor required for preimplantation development that protects the early embryo against DNA demethylation (Bortvin et al., 2004; Nakamura et al., 2007; Payer et al., 2003), is also found in presumptive PGCs (Saitou et al., 2002; Sato et al., 2002). However, STELLA is not required for germline development, as *stella* null mutants are viable and fertile (Payer et al., 2003). During putative PGC localization to the posterior region and prior to migration to the hindgut, only a subpopulation of TNAP-positive cells expressed *stella* (Saitou et al., 2002) while the majority (i.e., 80–100%) of *Blimp1*-expressing cells exhibited STELLA protein (Ohinata et al., 2005; Seki et al., 2007). At the same time, all STELLA-positive cells were reported to be TNAP- and *Blimp1*-positive (Ohinata et al., 2005; Saitou et al., 2002; Seki et al., 2007). Whether these relationships persist at later stages of PGC development, for example, as they migrate through the hindgut, is obscure.

To the best of our knowledge, there is no evidence demonstrating that the TNAP-, BLIMP1-, and STELLA-positive putative PGC populations actually translocate from the allantois/posterior primitive streak to the hindgut and gonads to contribute to the germ line. Although results from grafting experiments demonstrated that the posterior primitive streak/allantois of neural plate-stage conceptuses (~7.5 dpc) contributes TNAP-positive cells to the hindgut, whether these were derived from the posterior region's TNAP-positive, and not TNAP-negative, cell population is not known (Copp et al., 1986). Furthermore, if these cell populations represent the germ line, it remains unclear whether they are a homogeneous population that gives rise exclusively to germ cells, or whether they contribute to other cell types.

Nevertheless, despite the uncertainty of the precise nature of these markers vis-à-vis the PGCs, two studies have employed them to explore the timing of PGC lineage restriction. In the first, clonal analysis was used to fate-map a single cell per embryo (Lawson and Hage, 1994). Dextran labeling in conjunction with endogenous TNAP activity in the base of the allantois led to the conclusion that PGCs are specified as a distinct cell lineage at the neural plate stage, ~7.2 dpc, in the base of the allantoic bud. In the second study, genetic lineage tracing of the *Blimp1*-expressing population and identification of "specified PGCs" via STELLA localization led to a significantly different conclusion, i.e., that lineage restriction occurs prior to gastrulation, as early as ~6.25 dpc, in the small *Blimp1*-expressing population of the proximal epiblast (Ohinata et al., 2005). Differences in "markers" used may explain this major discrepancy, as *stella* was expressed only in a subpopulation of the posterior region's TNAP-positive cells (Saitou et al., 2002). In addition, clonal analysis might have missed the small specified PGC population claimed to exist at ~6.25 dpc.

Regardless of the discrepancies in these conclusions, the morphological endpoint in both studies was the allantois, prior to PGC translocation to the hindgut. As it is not known whether the putative PGCs scored in these studies would have ever translocated to the hindgut and ultimately colonized the gonads, it is possible that the scored TNAP- or STELLA-positive cells are not PGCs but actually part of a larger cell pool used to build the posterior region. Moreover, in the case of STELLA, previous expression and localization studies relied on whole mount analysis (Saitou et al., 2002) and limited sectional analysis (Sato et al., 2002), respectively. Therefore, STELLA's spatiotemporal pattern within the posterior region has not been examined in sufficient detail to conclude that STELLA exclusively localizes to the PGC trajectory or whether it may be found in other tissues of the posterior conceptus.

Recent evidence has suggested that the posterior primitive streak extends into the base of the allantois, where it establishes a precursor pool of cells, called the Allantoic Core Domain (ACD), used to build the allantois (Downs et al., 2009). The presence of the ACD in the allantois coincides with the localization of the putative PGCs within the allantois/posterior embryonic region (Anderson et al., 2000; Chiquoine, 1954; Ginsburg et al., 1990; Saitou et al., 2002). Like the PGCs, the ACD is positive for OCT-3/4 (Downs, 2008; Downs et al., 2009), which is found in relatively undifferentiated cells (Scholer et al., 1990). In addition, the ACD exhibits dynamic localization of extracellular matrix molecules COLLAGEN TYPE IV, E-CADHERIN, and PERLECAN (Daane et al., 2011; Mikedis and Downs, 2009), which are known to regulate many stem cell properties, such as proliferation and differentiation (reviewed in Kruegel and Miosge, 2010; Marthiens et al., 2010). Uniquely, only the region containing the ACD rescues allantoic elongation after grafting to microsurgically foreshortened allantoises in normal embryos and to genetically foreshortened allantoises in *Brachyury* (*T*) mutants (Downs et al., 2009). When the lipophilic tracer dye, DiI, was introduced into the ACD, labeled cells both persisted there and put forth a file of descendant cells through the allantoic midline that branched throughout the distal allantoic region (Downs et al., 2009). Finally, when ectopically grafted, some cells of the proximal allantois, and no other region, contributed to descendants of all three primary germ layers, suggesting the presence of a pluripotent population there (Downs and Harmann, 1997). Whether pluripotency was an intrinsic property of this tissue or due specifically to the presence of putative PGCs was not investigated.

Given the uncertainties concerning the true identity of the cells thought to be PGCs within the allantois, we decided to test the hypothesis that STELLA-positive cells may be found outside of the PGC trajectory, and/or are part of the ACD, the latter of which may be a larger, more general population used to build the posterior region of the mouse conceptus. Toward this end, we designed three experimental strategies. First, we localized STELLA to the mouse conceptus (Early Streak (ES)–12-s stages; ~6.75–9.0 dpc), focusing on the posterior region of the embryo and allantois. Second, to discover the fate of the ACD and surrounding regions, we fate-mapped the posterior region of the headfold-stage conceptus (~7.75–8.0 dpc), subdividing it into the distal allantois, distal ACD, proximal ACD, and intraembryonic posterior primitive streak (IPS). Third, to discover whether STELLA-positive cells in these regions contributed only to the hindgut, or whether they contributed to other cell types, we immunostained a subset of grafted chimeras to localize STELLA at the end of the culture period. Our results revealed that the STELLA-positive population is found in a variety of sites outside of the PGC trajectory, and that STELLA protein localized both within and outside of the cell nucleus. In addition, the proximal ACD and IPS, which together contained the majority of STELLA-positive cells, contributed to a range of tissues, both STELLA-positive and -negative, encompassing derivatives of the three primary germ layers within the posterior conceptus.

Materials and methods

Animal husbandry, embryo dissections, and staging

All animals were treated in accordance with Public Health Service (PHS) Policy on Humane Care and Use of Laboratory Animals (Public

Law 99–158) as enforced by the University of Wisconsin-Madison. Mouse conceptuses used in this study were derived from matings between B6CBAF1/J mice (The Jackson Laboratory, Bar Harbor, ME) or between B6CBAF1/J and ROSA26* *lacZ*/*lacZ* mice (Friedrich and Soriano, 1991; modified by Downs and Harmann, 1997). Conceptuses were dissected from time-mated females (Downs, 2006) and staged (Downs and Davies, 1993). For the STELLA localization study, conceptuses were dissected between ~6.75 and 9.0 dpc to provide stages ranging from ES to 12-s and were fixed for 2 h in 4% paraformaldehyde (PFA) at 4 °C. Gonads were dissected at 12.5 dpc, at which point the dissected conceptuses ranged from 26 to 28 tail somites; they were fixed for 23–24 h in 4% PFA at 4 °C. After fixation, specimens were rinsed in phosphate-buffered saline (PBS, Sigma), dehydrated in an increasing series of methanol/PBS, and stored indefinitely at −20 °C in absolute methanol.

Immunohistochemistry

Anti-STELLA immunohistochemistry was carried out in whole mount specimens as previously described (Downs, 2008). At each stage, at least 3 specimens were used. The primary antibody against STELLA (AF2566; 0.2 mg/mL stock; goat polyclonal; R&D Systems; Minneapolis, MN) and biotinylated donkey anti-goat IgG secondary antibody (sc-2042; 0.4 mg/mL stock; Santa Cruz Biotechnologies; Santa Cruz, CA) were both used at dilutions of 1/500. Anti-STELLA was visualized with diaminobenzoate chromagen (DAB; DAKO Corporation; Carpinteria, CA) applied at room temperature for 10 min, after which specimens were fixed in 4% PFA overnight at 4 °C. For the sectional analysis, specimens underwent standard dehydration and clearing. Then, specimens were embedded in paraffin wax for transverse or sagittal orientations, sectioned at a thickness of 6 micrometers (microns, μm), dewaxed, counterstained with hematoxylin, coverslipped, and analyzed. The reported localization patterns were consistent for all specimens analyzed at each stage, unless otherwise noted. Negative controls, in which the primary antibody was eliminated at the 4-s stage (N = 3 specimens), when staining signals were most abundant, verified antibody specificity (Fig. 1). STELLA signal was nuclear unless otherwise noted.

Microsurgical manipulations, whole embryo culture, and X-gal staining

Freshly dissected ROSA26* *lacZ*/+ conceptuses provided distal allantois, distal ACD, proximal ACD, and IPS grafts. Most grafts involved synchronous donor/host pairings but a few were stage-matched to within 2–4 h. Donor conceptuses were incubated for 2 min in trypsin/pancreatin (Downs and Harmann, 1997) and transferred to dissection medium (Downs, 2006). The four posterior subregions were then excised using long glass scalpels (Beddington, 1987). IPS isolation was similar to that previously described (Beddington, 1982; Tam and Beddington, 1987). Specifically, the IPS was isolated by opening up the conceptus to expose the posterior region and cutting along the site of amnion insertion, thereby separating the embryonic from the extraembryonic region. Then, the primitive streak, visualized as a groove along the anterior–posterior axis of the posterior embryo, was isolated by cutting along either side of the groove (Tam and Beddington, 1987). A final cut was made across the primitive streak, parallel to the cut along the site of amnion insertion, in order to isolate a piece of IPS approximately the size of the proximal ACD. Finally, the endoderm overlying the primitive streak was removed by micropipetting the isolated tissue repeatedly via a mouth aspirator, causing the endoderm to fall off of the isolated IPS. The proximal ACD was obtained by cutting along the site of insertion of the amnion, then the site of insertion of the allantois into the yolk sac, and finally between the allantois-associated extraembryonic visceral endoderm (AX) and proximal ACD. The remaining allantoic tissue was divided into distal ACD and distal allantois by cutting at the site where the allantois begins to decrease in width (Downs et al., 2009). The IPS and allantoic subregions were grafted into the IPS and proximal ACD, respectively, of the wildtype host conceptus' posterior region and cultured for 20–23 h in 1 mL culture medium (50% heat-inactivated rat serum) with 2 embryos per vial (Downs, 2006), distinguished by clipping the ectoplacental cone of one of the members of the pair with the scissor action of two 28-gauge hypodermic needles.

After culture, conceptuses were fixed in 4% PFA at 4 °C, rinsed 3 times in PBS, and stained with X-gal (Downs and Harmann, 1997) at 37 °C for 15–22 h to label donor-derived tissue. Conceptuses were dehydrated in an increasing series of methanol/PBS and stored indefinitely at −20 °C in absolute methanol. Later, conceptuses were rehydrated, and selected specimens were stained for STELLA. All specimens underwent standard dehydration and clearing, were embedded in wax for transverse orientations, sectioned at a thickness of 6 μm, and dewaxed. STELLA-immunostained and unstained specimens were counterstained with hematoxylin and Nuclear Fast Red, respectively, coverslipped, and analyzed.

Cell counts and statistical analyses

All cell counts in ex vivo and cultured specimens were obtained from sectioned material at 200 times magnification. For ex vivo specimens at headfold stages, STELLA-positive cells were scored based on localization to the proximal ACD/AX versus IPS/EVE (embryonic visceral endoderm), the boundary of which was defined by the site of amniotic insertion into the posterior region. For all STELLA-positive counts, all nuclei and/or brown cytoplasmic cell fragments were counted. Similarly, for quantification of graft contribution, all blue cells in any particular tissue were counted. Therefore, the numbers reported here are relative to each other, and may not represent absolute cell numbers. For all counts, averages were calculated from specimens exhibiting localization within each cell type, omitting those that were negative for this localization. For graft-derived contribution only, a maximum of 200 contributed cells were counted per cell type, and this value was then incorporated into the averages. Therefore, in some cases, the calculated averages underestimate contribution to a particular cell type, and are marked as such.

The statistical significance of the frequency of graft contribution to a particular cell type was calculated via a one-tailed exact binomial test (null hypothesis: a graft that does not contribute to a cell type under endogenous conditions will contribute to that cell type in the chimera approximately 0, i.e., less than 0.5, times). Because the largest group of chimeras was the 19 that received proximal ACD grafts, and 0.5 of 19 chimeras are expected to exhibit contribution to a cell type when the probability of contribution is 1/38, the probability of observing graft contribution was estimated as 1/39 (i.e., less than 1/38) for all graft types. All other analyses employed Student's two-tailed *t*-test. All calculations were made in Excel 2008, significance $p<0.05$.

For statistical analysis of graft integration along the length of the allantois, the length of the allantois was first determined by counting the number of sections containing allantoic tissue, and then multiplying by 6 μm/section to obtain a total length in microns. Regardless of graft type, all chimeric allantoises were similar in length ($p>0.1$), thereby verifying the validity of comparing allantoic contribution among the different graft types. The values for each specimen were normalized based on that specimen's total allantoic length such that 0 represented the base of the allantois and 1 represented the distal-most tip of the allantois. From these, the averages for each graft type were calculated.

Results

Specificity of STELLA antibody

Specificity of the antibody against STELLA was verified in histological sections at the 4-s stage by eliminating the primary antibody from the reaction ("minus primary antibody" control) (Figs. 1A, B). At this

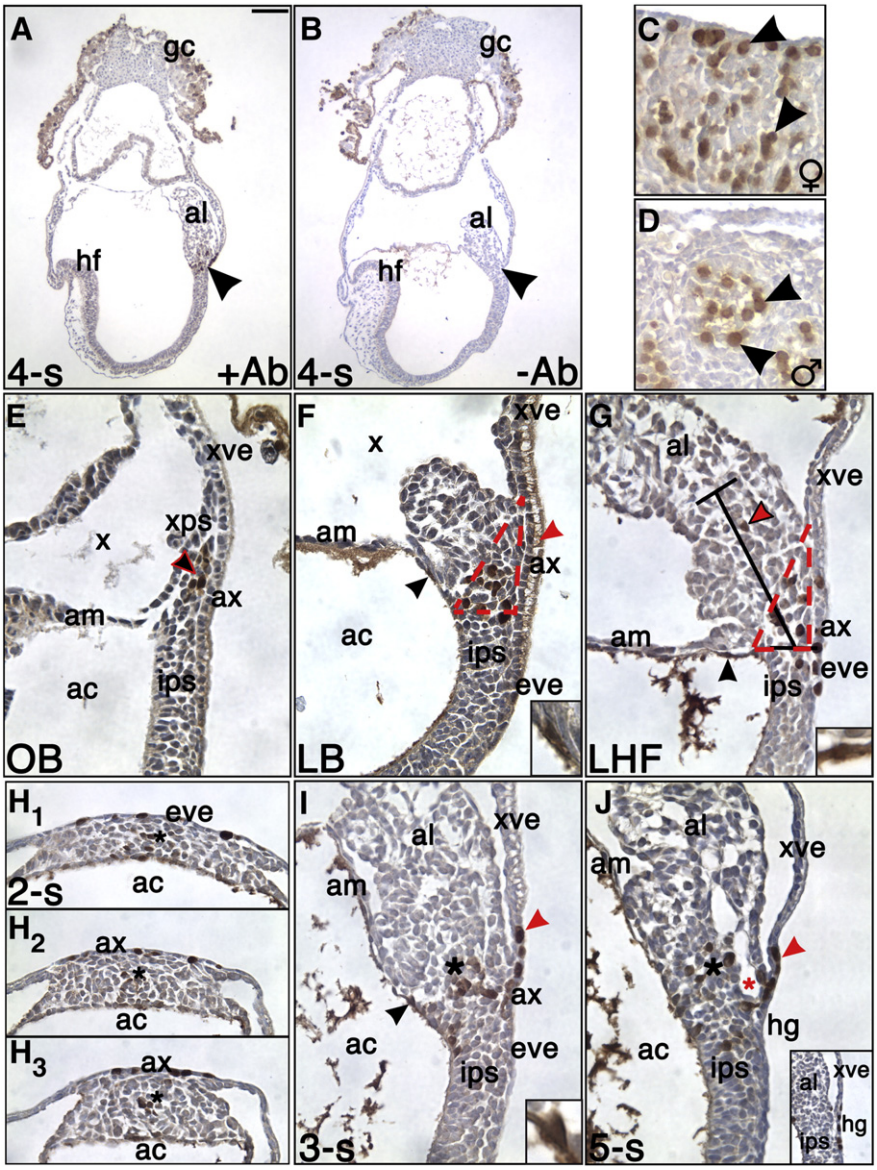

Fig. 1. Antibody specificity and STELLA in the posterior region during the early stages of allantoic development (Neural Plate/No Allantoic Bud (OB)–5-s; ~7.0–8.25 dpc). Unless otherwise indicated, all sections presented here and in subsequent figures are sagittal with anterior on the left and posterior on the right. STELLA is brown; unless otherwise noted, sections were counterstained in hematoxylin (blue color). (A) Staining with anti-STELLA (+Ab), 4-s stage. Arrowhead indicates STELLA-positive cells in the base of the allantois (al) and surrounding region. (B) Minus antibody control (−Ab), 4-s stage. Arrowhead indicates loss of STELLA in the allantois and surrounding region and thus, antibody specificity. Staining in the trophoblast giant cells (gc) and associated parietal endoderm may be spurious, and due to permeability associated with cell death during dissections. (C–D) Gonads, 12.5 dpc. Anti-STELLA detected exemplary germ cells (arrowheads) in developing female (♀; C) and male (♂; D) gonads. (E) OB stage (~7.0 dpc). A cluster of STELLA-positive cells (black arrowhead outlined in red) localized to the XPS (extraembryonic primitive streak, xps). (F) Late Bud (LB) stage (~7.5 dpc). A cluster of STELLA-positive cells expanded within the XPS (outlined by red dotted line) and into the IPS (intraembryonic primitive streak, ips). STELLA-positive cells in amniotic ectoderm (black arrowhead; higher magnification in inset) were occasionally observed at this stage. STELLA-positive vesicle in AX (allantois-associated extraembryonic visceral endoderm; ax) denoted by red arrowhead. (G) Late Headfold (LHF) stage (~8.0 dpc). A cluster of STELLA-positive cells localized to the proximal region of the Allantoic Core Domain, or ACD (outlined by red dotted line) as well as to the IPS, AX, and EVE (embryonic visceral endoderm, eve) overlying the IPS. Red arrowhead outlined in black marks the rare STELLA-positive cells that localized to a more distal region of the ACD, delineated by brackets, representing average length of 120 μm (Downs et al., 2009). STELLA-positive cell in amniotic ectoderm denoted by black arrowhead and displayed at higher magnification in inset. (H_{1-3}) 2-s stage (~8.25 dpc), transverse profile with ventral toward the top and dorsal toward the bottom of each panel. Sections represent: the IPS 18 μm below allantois (H_1), the base of the allantois at the embryonic/extraembryonic boundary (H_2), and 18 μm above the base of the allantois (H_3). Asterisk denotes approximate center of the IPS or ACD in each section. STELLA localization was dispersed across the dorsal-ventral axis of the posterior embryo (H_1) but most STELLA-positive cells were centrally confined within the ACD (H_{2-3}). STELLA-positive cells also localized to the EVE (H_1) and AX (H_{2-3}). (I–J) 3-s and 5-s stages (~8.25 dpc). STELLA-positive cells persisted in the ACD (black asterisk), IPS, EVE, and AX (I) as well as the hindgut (hg; J inset). Additional STELLA-positive cells localized to the ventral cuboidal mesothelium (VCM)-associated extraembryonic visceral endoderm (xve; red arrowhead). STELLA-positive cell in amniotic ectoderm denoted by black arrowhead and displayed at higher magnification in inset (I). Red asterisk (J) marks vessel of confluence. Other abbreviations: ac, amniotic cavity; am, amnion; hf, headfolds; and x, exocoelomic cavity. Scale bar in A = 200.0 μm (A–B), 26.7 μm (C–D), 24.8 μm (E–G, I, J), 8.3 μm (F inset), 8.4 μm (G inset), 34.2 μm (H_{1-3}), 7.3 μm (I inset), and 56.5 μm (J inset).

stage, strong STELLA-positive cells were detected in the conceptus' posterior region (Fig. 1A), where STELLA has been previously reported (Saitou et al., 2002; Sato et al., 2002). This staining was absent in the minus primary antibody controls (Fig. 1B). In addition, we further verified antibody specificity by confirming detection of STELLA-positive germ cells in female and male gonads at 12.5 dpc (Figs. 1C, D), when STELLA protein and *stella* mRNA localize to gonadal germ cells (Bowles et al., 2003; Sato et al., 2002). Further, as detailed below, nuclear STELLA was not detectable during gastrulation prior to the neural plate stage (~7.0 dpc), in accord with previous studies (Payer et al., 2006; Saitou et al., 2002). Also, the most abundant STELLA localization was confined to the posterior region of the mouse gastrula,

where protein and mRNA have been previously detected (Saitou et al., 2002; Sato et al., 2002). Finally, the number of STELLA-positive nuclei counted at the headfold stage for the fate-mapping studies, below, was also in general agreement with previous results (Seki et al., 2007).

Localization of STELLA along the putative PGC trajectory from the posterior region through the hindgut

Neural plate/No Allantoic Bud (OB)–Late Bud (LB) stages (~7.0–7.5 dpc)

Conceptuses as early as the Early Streak (ES) stage (~6.75 dpc) were examined; however, STELLA-positive nuclei were not detected in the conceptus until the neural plate/No Allantoic Bud (OB) stage (~7.0 dpc; Fig. 1E), in accord with a previous study reporting the initiation of *stella* mRNA expression in the posterior region at ~7.0 dpc (Saitou et al., 2002). Specifically, STELLA-positive cells formed a tight cluster within the putative extraembryonic extension of the primitive streak (XPS; Downs et al., 2009), where STELLA appeared to be localized to the nucleus. This is the site from which the ACD will be deployed, possibly via interaction with overlying allantois-associated extraembryonic visceral endoderm (AX; Downs et al., 2009).

From OB to Early Bud (EB) stages (~7.0–7.25 dpc), no nuclear STELLA-positive cells were detected outside of the allantois (Fig. 1E). However, by the LB stage (~7.5 dpc), the STELLA-positive population extended slightly across the embryonic–extraembryonic border into the IPS (Fig. 1F). In addition, in a few specimens, occasional STELLA-positive cells began to appear in the amniotic ectoderm closely associated with its site of insertion into the embryonic epiblast (Fig. 1F). In contrast to a previous report (Saitou et al., 2002), we never detected STELLA in the mesodermal component of the amnion. This discrepancy may be due to the ambiguities of whole mount analysis (Saitou et al., 2002), resolved here through examination of histological sections.

The allantois-associated extraembryonic visceral endoderm (AX; Downs, 2008; Downs et al., 2009), which overlies the extraembryonic primitive streak (XPS), exhibited occasional STELLA localization within cytoplasmic vesicles of varying sizes (Fig. 1F). Nuclei in the AX were negative.

Early Headfold (EHF)–5-s stages (~7.75–8.25 dpc)

During headfold stages (~7.75–8.0 dpc), the XPS expands to form the Allantoic Core Domain (ACD) along the allantoic midline (Fig. 1G), which persists in the proximal region of the allantois until at least 5-s (~8.25 dpc; Downs et al., 2009). Between headfold and 5-s stages, STELLA-positive cells were limited to a narrow band at the posterior embryonic/extraembryonic junction and dispersed throughout the dorsal–ventral width of tissue (Figs. 1G–J). STELLA-positive tissues included dorsal epiblast (Figs. 1H_1, I–J), allantois (Figs. 1G, H_2–J), embryonic visceral endoderm (EVE) overlying the IPS (Figs. 1G–H_1), and AX overlying the allantois (Figs. 1G, H_2–I).

During these stages, a small number of STELLA-positive cells consistently localized to the amniotic ectoderm adjacent to the IPS and proximal ACD (Figs. 1G, I). These STELLA-positive cells, potentially derived from a dorsal component of the IPS (suggested in Daane and Downs, 2011), appeared to be continuous with the STELLA-positive population in the posterior region. STELLA was not detected in the amniotic ectoderm after the 5-s stage (~8.25 dpc).

Within the allantois, STELLA-positive cells were largely confined to the proximal region of the ACD (Figs. 1G, H_2–J), where they formed a tight cluster within the midline (Fig. 1H_{2-3}). During headfold stages, this cluster occupied a "triangle" of tissue delineated by the site of insertion of the amnion and visceral yolk sac on the allantois, and the horizontal level of the amnion beneath that (Fig. 1G). At later stages, as the length of the AX and ACD decreased (Downs et al., 2009), the size of the triangle appeared to decrease as well, with STELLA-positive cells dispersing beyond this triangle (Fig. 1I) such that, by 5-s, STELLA-positive cells in the proximal ACD were less clustered and more scattered (Fig. 1J). Beyond the proximal ACD, an occasional STELLA-positive cell was observed in the distal ACD (Fig. 1G) but never in the extreme distal allantois at these stages.

In addition, from 1 to 5-s (~8.0–8.25 dpc), a small number of STELLA-positive cells (Figs. 1I, J) localized to the visceral yolk sac's extraembryonic visceral endoderm (XVE) associated with the proximal ventral wall of the allantois, called the ventral cuboidal mesothelium (VCM; Daane et al., 2011). This small segment of visceral endoderm, lying distal to the AX, exhibited a squamous morphology similar to the AX and EVE instead of the classical vesiculated morphology of yolk sac XVE (Daane et al., 2011).

By 4-s (~8.25 dpc), many allantoic STELLA-positive cells appeared to be closely associated with the VCM (Daane et al., 2011), and the underlying vessel of confluence (VOC; Fig. 1J), which is the site of amalgamation between the nascent arterial systems of the allantois, yolk sac and fetus (Daane et al., 2011; Downs et al., 1998). In addition, as the hindgut formed, STELLA-positive cells were found within its endoderm (Fig. 1J).

6–8-s stages (~8.5 dpc)

By 6–8-s (~8.5 dpc), concomitant with the apparent loss of the ACD (Downs et al., 2009), a limited number of STELLA-positive cells were now found within the proximal allantois (Fig. 2A_3). Some of these cells were closely associated with the VCM and the underlying vessel of confluence (Fig. 2A_3). In addition, single or small clusters of STELLA-positive cells were now usually observed in more distal regions of the allantois (Figs. 2B, C_5), though an occasional specimen lacked these more distal cells. The presence of distal STELLA-positive cells is consistent with the proximal-to-distal movement of cells within the allantois (Downs and Harmann, 1997; Downs et al., 2009).

During this period, the hindgut invagination was forming a tube (Fig. 2C_{2-3}). STELLA-positive cells were observed in visceral endoderm flanking the future hindgut tube (Fig. 2C_1). Within the tube itself, the majority of STELLA-positive cells localized to ventral endoderm, near the omphalomesenteric artery (Figs. 2A_2–B, C_{2-3}); however, a few STELLA-positive cells were found within dorsal hindgut endoderm, particularly toward its caudal end (Figs. 2A_1, C_3).

A range of STELLA-positive cells persisted in the posterior mesoderm of the developing tailbud (Figs. 2A_2, C_4), some of which contained relatively reduced anti-STELLA reactivity compared to STELLA-positive cells in the hindgut. In addition, a few STELLA-positive cells were occasionally observed within distal posterior surface ectoderm (Fig. 2C_{3-4}), including a small population that persisted within the surface ectoderm near the allantoic–amniotic junction (Fig. 2A_{1-2}).

9–12-s stages (~ 8.75–9.0 dpc)

By 9-s (~8.75 dpc), hindgut STELLA-positive cells were confined to its ventral side (Figs. 2D–E_1). Outside of the hindgut, occasional STELLA-positive cells localized to the surface ectoderm (Figs. 2D, E_2) as well as to posterior mesoderm, both general mesenchyme (Fig. 2D) and, occasionally, mesoderm of the somatopleure (data not shown).

Intriguingly, in some specimens at 10–12-s (~9.0 dpc), a population of STELLA-positive cells localized to the surface ectoderm of the ventral tailbud just above the caudal terminal end of the hindgut to a site that appeared to be undergoing an epithelial-to-mesenchymal transition (Fig. 2E_3). This site is likely the early ventral ectodermal ridge, a remnant of the primitive streak that forms at ~9.0 dpc and is required for extending the tail posteriorly (Goldman et al., 2000; Grüneberg, 1956; Ohta et al., 2007; Tam and Tan, 1992; Wilson and Beddington, 1996).

Within the allantois, occasional STELLA-positive cells appeared sporadically either as a single cell or as a small cluster of cells throughout the length of the allantois, both within its core (data not shown) and on its mesothelial surface (Fig. 2E_3).

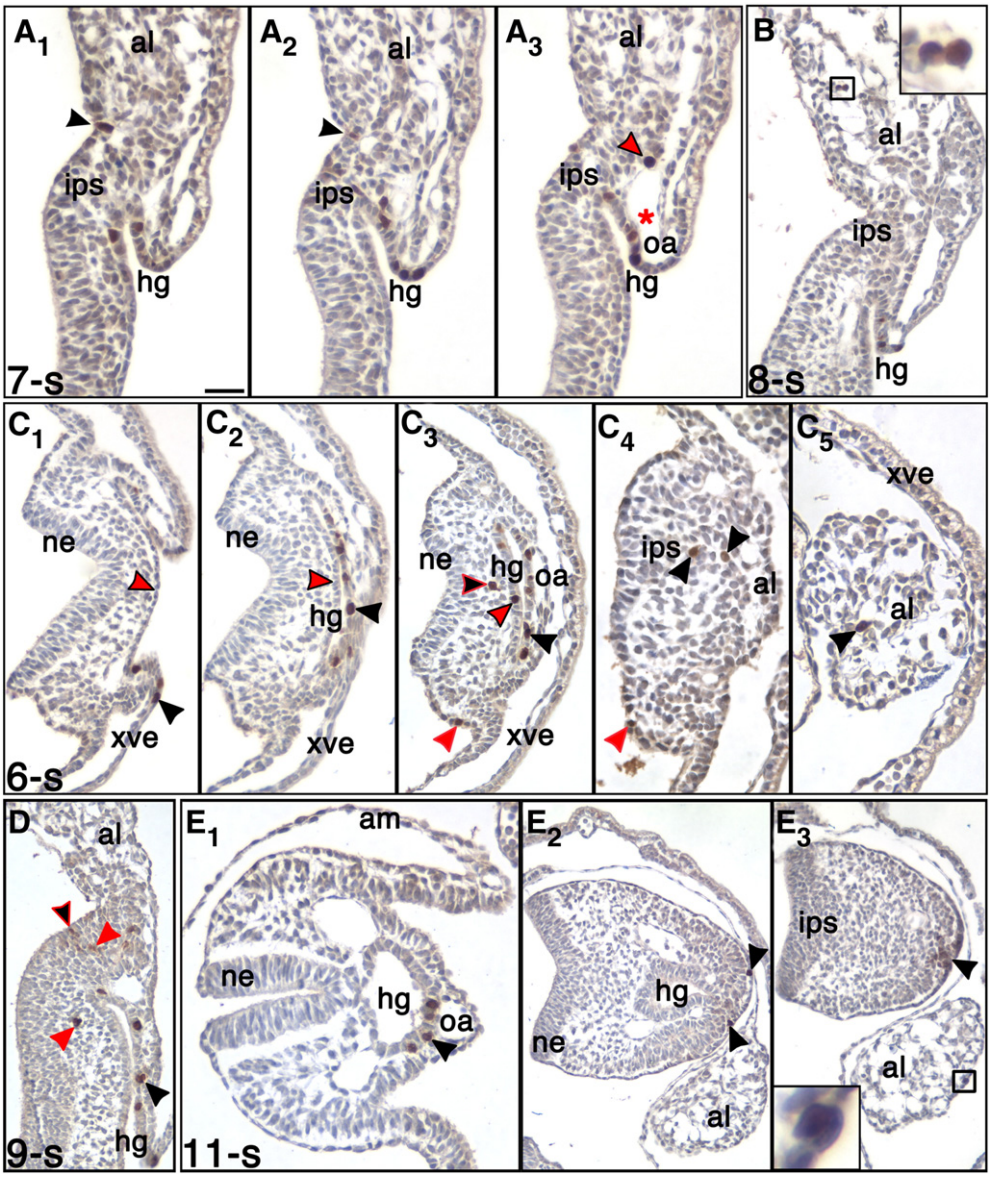

Fig. 2. STELLA during early hindgut tube formation (6–12-s; ~8.5–9.0 dpc). (A_{1-3}) 7-s stage (~8.5 dpc). STELLA-positive cells localized to the dorsal (A_1) and ventral (A_{1-3}) hindgut as well as at the site of amniotic insertion at the embryonic–extraembryonic junction (black arrowheads in A_{1-2}), IPS (A_{2-3}), and near the vessel of confluence in the allantois (red arrowhead outlined in black, A_3). Red asterisk marks vessel of confluence. (B) 8-s stage (~8.75 dpc). A cluster of STELLA-positive cells localizing to the midregion of the allantois (box; higher magnification in inset). (C_{1-5}) 6-s stage (~8.5 dpc), transverse profile with dorsal to the left and ventral to the right of each panel. This sequence begins at the hindgut opening and proceeds posteriorly toward the allantois. (C_1) 18 μm below the anterior-most segment of closed hindgut tube. STELLA-positive cells (black arrowhead) localized to the endoderm at the leading edge of the open hindgut. Note absence of STELLA-positive cells in presumptive dorsal hindgut endoderm (red arrowhead outlined in black). (C_2) Anterior-most segment of closed hindgut tube. STELLA-positive cells localized to the ventral (black arrowhead), but not dorsal (red arrowhead outlined in black), side. (C_3) More posteriorly (24 μm posterior to the anterior-most segment of the closed hindgut tube, and 36 μm anterior to the end of the hindgut tube), STELLA-positive cells primarily localized to the ventral hindgut (black arrowhead), but some also localized to the dorsal hindgut (red arrowhead outlined in black). In addition, STELLA-positive cells localized to the posterior mesenchyme (black arrowhead outlined in red) and posterior dorsal surface ectoderm (red arrowhead). (C_4) 12 μm posterior to the end of the hindgut tube. STELLA-positive cells localized outside of the hindgut to surface ectoderm (red arrowhead) and in the IPS near the allantois (black arrowhead). (C_5) 132 μm and 144 μm posterior to base of the allantois and the end of the hindgut, respectively. STELLA-positive cell (black arrow) in the allantois. (D) 9-s stage (~8.75 dpc). STELLA localization in the ventral hindgut (black arrowhead), posterior loose mesenchyme (red arrowheads), and surface ectoderm (black arrowhead stroked in red). (E_{1-3}) 11-s stage (~9.0 dpc), transverse profile. The tail has turned, and the allantois has shifted its position to lie in the posterior ventral midline. These sections were taken at the level of the closed hindgut tube anterior (E_1) and posterior (E_{2-3}) to the allantoic insertion into the tailbud. (E_1) STELLA-positive cells (black arrowhead) localize to the ventral hindgut. (E_2) STELLA-positive cells (black arrowheads) localize near the surface ectoderm of the tailbud, 18 μm below the posterior end of hindgut. (E_3) Anti-STELLA reactivity (black arrow) in the ventral ectoderm ridge of the posterior embryo, 12 μm above the end of the posterior hindgut. STELLA also localized to the allantois (box; higher magnification in inset), 60 μm from the site of posterior allantoic attachment to the embryo. Other abbreviations: ne, neurectoderm; and oa, omphalomesenteric artery. Scale bar in $A_1 = 27.3$ μm (A_{1-3}), 35.7 μm (B), 9.0 μm (B inset), 37.8 μm (C_{1-3}), 26.1 μm (C_4), 25.1 μm (C_5), 42.3 μm (D), 30.6 μm (E_1), 55.3 μm (E_{2-3}), and 8.3 μm (E_3 inset).

Localization of STELLA to tissue outside of the presumptive PGC trajectory

Yolk sac blood islands

From the initiation of yolk sac blood island formation at the neural plate stage (~7.0 dpc) through the end of our study at 12-s (~9.0 dpc), STELLA was detected in most specimens within small numbers of putative blood cells and/or blood cell precursors within the blood islands (Fig. 3A, inset). Localization was not nuclear, but restricted to small cytoplasmic vesicles.

Extraembryonic visceral endoderm (XVE) of the yolk sac

From streak through neural plate stages (~6.75–7.5 dpc), occasional cytoplasmic vesicles of varying sizes within the XVE contained STELLA (Fig. 1F and data not shown). Nuclei were negative. By headfold stages

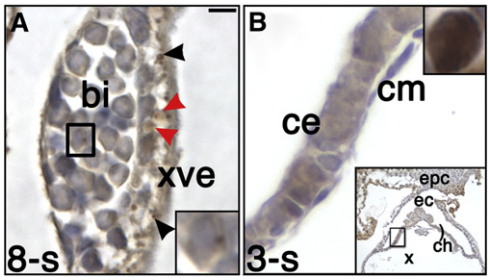

Fig. 3. STELLA localization in the extraembryonic visceral yolk sac and chorionic ectoderm. (A) 8-s stage (~8.75 dpc), visceral yolk sac blood islands (bi). A single hematopoietic cell (outlined with black box; higher magnification in lower right inset) with a cytoplasmic dot of STELLA staining within a yolk sac blood island. Dark, dense STELLA (black arrowheads) and larger, transparent-looking STELLA (red arrowheads) localized within vesicles of the extraembryonic visceral endoderm (xve) of the visceral yolk sac. (B) 3-s stage (~8.25 dpc), chorionic ectoderm (ce). Chorionic ectoderm, from portion of chorion (ch) highlighted in lower right inset, contains diffuse STELLA, and ambiguous nuclear staining (compare chorionic ectoderm staining with robust STELLA-positive nucleus from AX within the same specimen, upper right inset). Other abbreviations: cm, chorionic mesoderm; ec, ectoplacental cavity; and epc, ectoplacental cone. Scale bar in A = 7.2 μm (A), 3.0 μm (A inset), 8.3 μm (B), 3.6 μm (B upper right inset), and 100.0 μm (B lower right inset).

Table 1
Number of STELLA-positive nuclei localizing to various tissues in the posterior region of ex vivo conceptuses at headfold stages (~7.75–8.0 dpc).

Tissue	No. STELLA-positive conceptuses/total no. conceptuses examined	Average[a] no. of STELLA-positive nuclei (sem)
Total posterior region[b]	10/10	100.0 (10.3)
Proximal ACD	10/10	41.6 (4.1)
Distal ACD	3/10	2.3 (0.9)
AX	7/10	8.1 (1.8)
IPS	10/10	31.1 (2.8)
EVE	8/10	13.6 (3.4)
Amniotic ectoderm	10/10	10.0 (1.9)

No STELLA-positive cells localized to distal allantois.
Abbreviations: no, number; and sem, standard error of the mean.
[a] Average within each tissue calculated from only those specimens containing STELLA-positive cells in that tissue.
[b] Includes tissues listed in this chart but not chorionic ectoderm or yolk sac blood islands, in which nuclei were not strongly positive (see Results).

(~7.75–8.0 dpc), the majority of XVE cells contained vesicles of anti-STELLA reactivity (Fig. 3A). This pattern of localization persisted through the 12-s stage (~9.0 dpc).

Chorionic ectoderm

We also detected diffuse STELLA staining in chorionic ectoderm from OB through 8-s stages (~7.0–8.75 dpc; Fig. 3B), when trophoblast stem cells are found here (Uy et al., 2002). No other tissues exhibited this haze of STELLA staining, which seemed to be neither strongly nuclear nor strongly cytoplasmic. Intensity of staining varied along the length of the chorion in an inconsistent manner, but even the most intensely stained cells were relatively less intense than the strong STELLA staining in the posterior region within any given specimen (compare Fig. 3B to upper right inset).

Fate-mapping the posterior region at headfold stages (~7.75–8.0 dpc)

Previous investigators placed the timing of PGC restriction to ~7.2 dpc at the latest, prior to the formation of the hindgut invagination at 4-s (~8.25 dpc). However, results presented here indicate that between these stages, many STELLA-positive cells persisted outside of the posterior endoderm (Figs. 1F–I). On the basis of this observation, we hypothesized that not all STELLA-positive cells contributed to the putative PGC population in the hindgut. To test this, we grafted STELLA-rich regions to find out whether STELLA-positive cells contributed to tissues other than the hindgut. Headfold-stage conceptuses were selected for several reasons. First, the Allantoic Core Domain (ACD) is thought to form at this time, and would thus be in its most primitive state (Downs et al., 2009). Second, we wanted to know whether the ACD contributed only to the allantois, or whether it also contributed to the fetus. Third, if the ACD's STELLA-positive PGC population formed a restricted lineage there, then all STELLA-positive cells should contribute only to the hindgut at the end of the culture period.

We first counted the number of STELLA-positive cells in the posterior region (Table 1). On average, the headfold-stage posterior region contained 100.0 STELLA-positive cells (Table 1), in accord with previous numbers of *stella*-EGFP-positive cells counted via confocal analysis (Seki et al., 2007).

Next, the posterior region of ROSA26* *lacZ*/+ hemizygous transgenic donor conceptuses was subdivided into the distal allantois, distal ACD, proximal ACD, and intraembryonic posterior streak (IPS; Fig. 4A). The distal ACD contained the allantois' ventral cuboidal mesothelium (VCM), while the proximal ACD contained the dorsal cuboidal mesothelium (DCM; Fig. 4), each of which has been shown to exhibit distinct permeability and molecular profiles (Daane et al., 2011). Each subregion was placed synchronously into the embryonic–extraembryonic junction of a non-transgenic host conceptus (Fig. 4B). Specifically, the proximal ACD and IPS were orthotopically

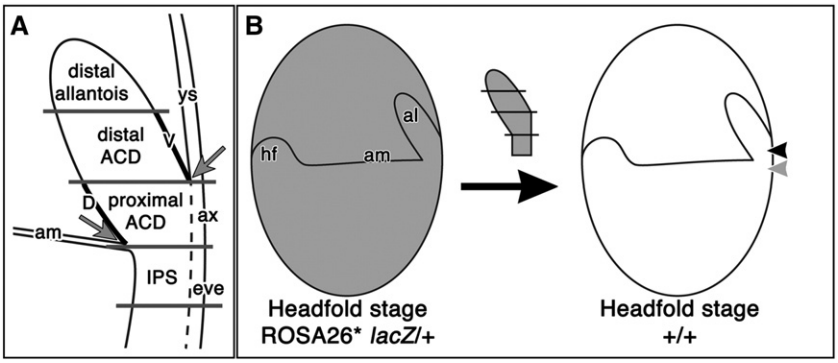

Fig. 4. Fate-mapping the posterior region via synchronous (approximate) orthotopic grafting. (A) The headfold-stage posterior region was divided into four subregions: distal allantois, distal ACD, proximal ACD, and IPS. Site of insertion of amnion (am) was used to separate the (extraembryonic) allantoic tissue from embryonic tissue. Site of insertion of the allantois into the visceral yolk sac (ys) was used to define the boundary between proximal and distal ACD. Overlying allantois-associated extraembryonic visceral endoderm (ax) and embryonic visceral endoderm (eve), both of which are delineated by the dotted line, were removed from the proximal ACD and IPS, respectively. The proximal ACD contained the dorsal cuboidal mesothelium (D), and the distal ACD contained the ventral cuboidal mesothelium (V). (B) Donor posterior regions from headfold-stage ROSA26* *lacZ*/+ hemizygous donor conceptuses were removed and isolated into four subregions (see A). Allantoic subregions and the IPS were synchronously grafted into a non-transgenic host's proximal ACD (black arrowhead) and IPS (gray arrowhead), respectively. Other abbreviations: al, allantois; and hf, headfolds.

grafted into the host's proximal ACD and IPS, respectively; the distal ACD and distal allantois were approximate-orthotopically grafted into the host's proximal ACD. After culture, X-gal staining, and in many cases, immunostaining for STELLA, chimeras (9–12-s; ~8.75–9.0 dpc) were analyzed for graft contribution to embryonic and extra-embryonic tissues (Fig. 5).

No differences in the number of STELLA-positive nuclei were observed among equivalently staged ex vivo (uncultured) specimens, unoperated culture controls, and host-derived STELLA-positive cells in the operated chimeras (Fig. 5I; $p>0.1$ for all comparisons). Thus, the culture conditions used in this study were appropriate for normal STELLA development. Moreover, the X-gal-stained ROSA26* *lacZ*/+ unoperated culture controls and non-transgenic ex vivo specimens contained similar numbers of total STELLA-positive cells ($p=0.4949$; Table 2), showing that X-gal staining does not compromise visualization of STELLA via immunohistochemistry.

Frequency of chimerism is summarized in Table 3. Only those chimeras with well-integrated graft contribution and normal morphology were used for fate analyses (Table 4–7). Because each chimera received a full donor subregion, graft contribution to a specific cell type could be

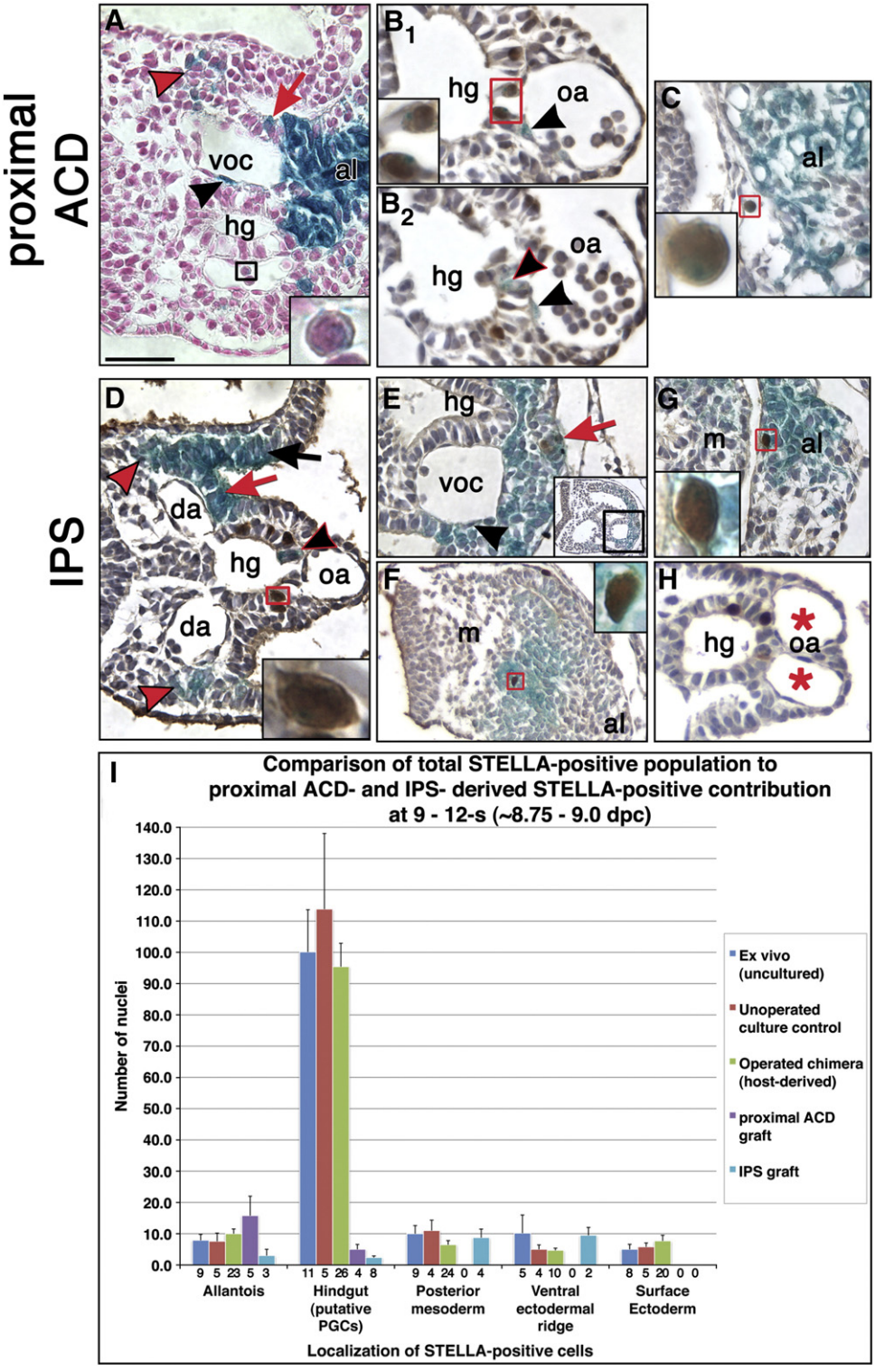

Table 2
Number of STELLA-positive nuclei localizing to various tissues in the posterior region of ex vivo (uncultured) conceptuses and cultured ROSA26* *lacZ*/+ unoperated controls at 9–12-s (~8.7–9.0 dpc).

Tissue	Ex vivo conceptuses		Cultured ROSA26* *lacZ*/+ unoperated controls	
	No. STELLA-positive conceptuses/total no. conceptuses examined	Average[a] no. of STELLA-positive nuclei (sem)	No. STELLA-positive conceptuses/total no. conceptuses examined	Average[a] no. of STELLA-positive nuclei (sem)
Total posterior region[b]	11/11	123.0 (17.2)	3/3	153.7 (59.2)[c]
Hindgut	11/11	100.1 (13.5)	3/3	106.7 (32.7)[c]
Allantois	9/11	7.9 (1.9)	3/3	8.0 (4.0)[c]
Posterior mesoderm[d]	9/11	10.0 (2.6)	3/3	11.7 (5.0)[c]
Surface ectoderm	8/11	5.0 (1.6)	3/3	7.7 (4.1)[c]
Ventral ectodermal ridge	5/6[e]	10.2 (5.8)	3/3	19.7 (14.2)[c]

One ex vivo specimen (11-s) had 1 STELLA-positive nucleus in the visceral yolk sac endoderm near the site of hindgut closure.
Abbreviations: no, number; and sem, standard error of the mean.
[a] Average within each tissue calculated from only those specimens containing STELLA-positive cells in that tissue.
[b] Includes tissues listed in this chart but not chorionic ectoderm or yolk sac blood islands, in which nuclei were not strongly positive (see Results).
[c] Comparison of ex vivo conceptuses and cultured ROSA26* *lacZ*/+ unoperated controls via Student's *t*-test revealed no differences in STELLA-positive populations within total posterior region ($p=0.4949$), hindgut ($p=0.8329$), allantois ($p=0.9780$), posterior mesoderm ($p=0.7583$), surface ectoderm ($p=0.4710$), and ventral ectodermal ridge ($p=0.4922$).
[d] Includes cells from general loose mesenchyme and mesoderm associated with somatopleure; STELLA-positive cells were never observed in splanchnopleure.
[e] 6 out of 11 specimens (10–12-s) contained a ventral ectodermal ridge.

analyzed not only by the number of cells contributed to individual tissues, but also by the frequency of contribution among multiple chimeras, thereby allowing detection of small contributions. Statistically significant results (i.e., $p<0.05$), along with average cell contribution (Table 8), are reported below.

The distal allantois (Tables 4, 8) contributed primarily to the allantois with additional contribution to the endothelium of both the omphalomesenteric artery and the visceral yolk sac. A subset of distal allantois-derived chimeras was immunostained for STELLA, and graft-derived STELLA-positive cells were not detected (Table 4).

The distal ACD (Tables 5, 8) contributed extensively to the allantois, with additional contribution to the endothelium of the omphalomesenteric artery and vessel of confluence. The distal ACD also contributed to visceral yolk sac endothelium and hematopoietic cells within yolk sac blood islands. Within the subset of distal ACD-derived chimeras immunostained for STELLA, only one chimera exhibited a graft-derived STELLA-positive cell in the hindgut, but this frequency of chimerism was not statistically significant (Table 5).

The proximal ACD (Tables 6, 8) contributed extensively to the allantois (Fig. 5C). Additionally, the proximal ACD contributed to the endothelium of the dorsal aortae, omphalomesenteric artery (Fig. 5B), and vessel of confluence (Fig. 5A); circulating hematopoietic cells of the posterior conceptus (Fig. 5A, inset); splanchnopleure, which covers the ventral surface (Fig. 5A); ventral hindgut (Fig. 5B); and posterior mesoderm (Fig. 5A). Intriguingly, contribution to hematopoietic cells was observed only in chimeras with contribution to posterior arterial endothelium (Table 6), from which hematopoietic cells are thought to bud (Boisset et al., 2010; Chen et al., 2009). The proximal ACD also demonstrated statistically significant contribution to visceral yolk sac endothelium and amnion, the latter of which was only observed at sites where the amnion was closely associated with graft-derived allantoic tissue. Furthermore, 1 out of 19 chimeras exhibited a double host-derived omphalomesenteric artery (Table 6 and data not shown).

A subset of proximal ACD-derived chimeras was immunostained for STELLA (Table 6). In these, the proximal ACD contributed STELLA-positive cells to the hindgut (Fig. 5B$_1$; Table 8), though the size of this contribution was a fraction of the total STELLA-positive hindgut population in unoperated controls ($p=0.0055$; Fig. 5I). In addition, the proximal ACD contributed STELLA-positive cells to the allantois (Fig. 5C) in numbers that were similar to those observed in the allantois of unoperated controls ($p=0.2174$; Fig. 5I). Total graft-derived STELLA-positive contribution (16.8 cells; Table 8) was less than the total STELLA-positive

Fig. 5. Proximal ACD and IPS contribute STELLA-positive and STELLA-negative cells to the posterior conceptus (9–12-s; ~8.75–9.0 dpc). All sections are transverse profiles with ventral on the right and dorsal on the left of each panel. (A) 10-s. Proximal ACD graft contributed to splanchnopleure (red arrow), endothelium of the vessel of confluence (voc; black arrowhead), posterior mesoderm (red arrowhead outlined in black), and circulating hematopoietic cell (black box; higher magnification within inset). Specimen counterstained with Nuclear Fast Red (pink color). (B$_{1-2}$) 11-s. Proximal ACD graft contributed to endothelium of the omphalomesenteric artery (oa; B$_{1-2}$, black arrowhead) as well as to STELLA-positive cells (B$_1$, red box; higher magnification within inset) and STELLA-negative cells (B$_2$, black arrowhead outlined in red) in the ventral hindgut. (C) 10-s. Proximal ACD graft contributed to the allantois, including STELLA-positive cells (red box, higher magnification within inset). (D) 11-s. IPS graft contributed to splanchnopleure (red arrow), somatopleure (black arrow), STELLA-positive cells (red box; higher magnification within inset) and STELLA-negative cells (black arrowhead outlined in red) within ventral hindgut, and posterior mesoderm (red arrowheads outlined in black). (E) 11-s. Black box within lower magnification inset (lower right) is magnified in this panel. IPS graft contributed to STELLA-positive and -negative cells in ventral ectodermal ridge (red arrow) as well as to endothelium of the vessel of confluence (black arrowhead). (F) 9-s. IPS graft contributed to posterior mesoderm, including STELLA-positive cells (red box, higher magnification within inset). (G) 9-s. IPS graft contributed to the allantois, including STELLA-positive cells (red box, higher magnification within inset). (H) 10-s. Host-derived double omphalomesenteric artery (red asterisks) in chimera that received IPS graft. Graft contribution occurred posterior to this section. (I) Comparison of total STELLA-positive population in ex vivo specimens, unoperated controls, and operated chimeras (host-derived STELLA-positive cells only) to proximal ACD- and IPS-derived STELLA-positive contribution at 9–12-s (~8.75–9.0 dpc). Only those proximal ACD or IPS grafts that exhibited STELLA-positive contribution to a particular cell type were included in this analysis. No STELLA-positive cells were observed in the splanchnopleure. STELLA-positive populations in the allantois, hindgut, posterior mesoderm (loose mesenchyme and somatopleure-associated mesoderm), ventral ectodermal ridge, and surface ectoderm were similar in ex vivo specimens when compared to unoperated culture controls ($p=0.9288$, $p=0.6011$, $p=0.8273$, $p=0.4614$, and $p=0.7344$, respectively) and operated chimeras ($p=0.4464$, $p=0.7466$, $p=0.1964$, $p=0.1994$, and $p=0.3748$, respectively). In addition, STELLA-positive populations in these tissues were similar between unoperated culture controls and operated chimeras ($p=0.5018$, $p=0.3632$, $p=0.2083$, $p=0.8396$, and $p=0.6055$, respectively). Proximal ACD grafts contributed similar numbers of STELLA-positive cells to the allantois as found in ex vivo specimens ($p=0.1208$), unoperated controls ($p=0.2174$), and operated host chimeras ($p=0.1617$). IPS grafts contributed similar numbers of STELLA-positive cells to the allantois and posterior mesoderm as ex vivo specimens ($p=0.1921$ and $p=0.7850$, respectively), unoperated controls ($p=0.2672$ and $p=0.6501$), and operated host chimeras ($p=0.1172$ and $p=0.5242$). IPS grafts also contributed similar numbers of STELLA-positive cells to the ventral ectodermal ridge compared to ex vivo specimens ($p=0.9456$) and unoperated controls ($p=0.1605$), but more cells compared to operated chimeras ($p=0.0305$). Proximal ACD and IPS grafts contributed fewer STELLA-positive cells to the hindgut compared to ex vivo specimens ($p=0.0011$ and $p<0.0001$, respectively), unoperated controls ($p=0.0055$ and $p<0.0001$, respectively), and operated host chimeras ($p<0.0001$ for both graft types). All statistical calculations based on Student's *t*-test at a 0.05 significance level. Error bars represent standard error of the mean (sem); number below each graph bar represents sample size. Other abbreviations: da, dorsal aortae. Scale bar in A = 33.3 μm (A), 7.5 μm (A inset), 34.4 μm (B$_{1-2}$), 16.2 μm (B$_1$ inset), 50.0 μm (C–E, G), 9.6 μm (C inset), 10.0 μm (D inset), 254.4 μm (E inset), 76.0 μm (F), 15.0 μm (F inset), 10.1 μm (G inset), and 43.2 μm (H).

Table 3
Frequency of experimental chimeras.

Grafted tissue	No. expts	No. injected conceptuses	No. neg. grafts (%)	No. grafts unincorporated (%)	No. poorly incorporated grafts/abnormal chimeras (%)	No. normal chimeras (%)	Major type(s) of tissue colonized
Distal allantois	9	19	1 (5.3)	5 (26.3)	3 (15.8)	10 (52.6)	Allantois
Distal ACD	11	27	4 (14.8)	2 (7.4)	11 (40.7)	10 (37.0)	Allantois; posterior vasculature
Proximal ACD	10	28	2 (7.1)	2 (7.1)	5 (17.9)	19 (67.8)	Multiple
IPS	5	15	0	0	3 (20.0)	12 (80.0)	Multiple

Abbreviations: expts, experiments; neg, negative; and no, number.

population present in the headfold-stage proximal ACD prior to grafting (41.6 cells; Table 1; $p = 0.0018$).

All intraembryonic posterior streak (IPS) grafts (Tables 7, 8) contributed extensively to the posterior mesoderm as well as to somatopleure and splanchnopleure (Fig. 5D), which cover the lateral and mid-regions, respectively, of the ventral body surface at these stages. The IPS also contributed to the allantois (Fig. 5G), endothelium of the dorsal aortae, omphalomesenteric artery, and vessel of confluence (Fig. 5E); ventral hindgut (Fig. 5D); and surface ectoderm. Furthermore, based on the few specimens in which the ventral ectodermal ridge could be identified, the IPS gave rise to it (Fig. 5E). The IPS also demonstrated statistically significant contribution to the visceral yolk sac endothelium. Finally, 2 out of 12 chimeras exhibited a double omphalomesenteric artery that was derived from the host, not the donor IPS (Table 7; Fig. 5H).

IPS chimeras, all of which were stained for STELLA, exhibited contribution of STELLA-positive cells to the putative PGCs in the hindgut (Fig. 5D), though this contribution was significantly smaller than the average STELLA-positive hindgut population in unoperated controls ($p<0.0001$; Fig. 5I). In numbers that were similar to those observed in unoperated controls (Fig. 5I), other STELLA-positive contribution was observed in the allantois ($p = 0.2672$; Fig. 5G), posterior mesoderm ($p = 0.6501$; Fig. 5F), and the ventral ectodermal ridge ($p = 0.1605$; Fig. 5E). Total graft-derived STELLA-positive contribution (8.3 cells; Table 8) was less than the total STELLA-positive population present in the headfold-stage IPS prior to grafting (31.1 cells; Table 1; $p<0.0001$).

Contribution to the allantois varies by graft type

Previous results suggested that the allantois might grow by a stacking mechanism (Downs and Harmann, 1997; Downs et al., 1998; Kinder et al., 1999), in which distal allantoic cells are the oldest and proximal cells are the youngest; differentiation then occurs by regional cues. Although all regions of the posterior conceptus contributed to the allantois, we hypothesized that graft contribution along the length of the allantois would vary by graft type. Because no significant differences were observed in allantoic length among chimeras that received distal allantois, distal ACD, proximal ACD, or IPS ($p>0.1$ for all comparisons), we normalized the placement of allantoic sections within each chimera based on total allantoic length so that 0 represented the proximal-most allantoic section attached to the posterior embryo while 1 represented the distal-most section attached to the chorion. This analysis revealed that graft contribution varied along the length of the allantois based on graft type (Fig. 6).

Table 4
Distribution of cells derived from distal allantois grafts in chimeras.

Tissue		Chimera number									
		1	2	3	4	5	6	7	8	9	10
Allantois (Total)[a]		+	+	+	+	+	+	+	+	+	+
Vessel endothelium	Dorsal aortae	–	–	–	–	–	–	–	–	–	2
	Omphalomesenteric artery	–	–	–	–	–	–	–	–	32	36
	Vessel of confluence	–	–	–	–	–	–	–	–	–	21
	Yolk sac	–	–	–	–	–	–	–	44	148	5
Hematopoietic cells	Posterior embryo[b]	–	–	–	–	–	–	–	–	–	3
	Yolk sac blood islands	–	–	–	–	–	–	–	–	–	8
Other tissues of the posterior embryo	Hindgut (Total)[a]	–	–	–	–	–	–	–	–	–	–
	Posterior mesoderm (Total)[a, c]	–	–	–	–	–	–	–	–	–	2
	Somatopleure	–	–	–	–	–	–	–	–	–	–
	Splanchnopleure	–	–	–	–	–	–	–	–	–	–
	Surface ectoderm (Total)[a]	–	–	–	–	–	–	–	–	–	–
	Ventral ectodermal ridge (Total)[a]	–	–	–	–	–	–	–	–	–	–
Other extraembryonic tissues	Yolk sac XVE	–	–	–	–	–	–	–	–	–	–
	Yolk sac mesothelium	–	–	–	–	–	–	–	–	–	–
	Amnion	–	–	–	–	–	–	–	–	–	–
STELLA–positive cells only	Hindgut	n/d	n/d	n/d	n/d	n/d	n/d	n/d	n/d	–	–
	Posterior mesoderm[c]	n/d	n/d	n/d	n/d	n/d	n/d	n/d	n/d	–	–
	Surface ectoderm	n/d	n/d	n/d	n/d	n/d	n/d	n/d	n/d	–	–
	Ventral ectodermal ridge	n/d	n/d	n/d	n/d	n/d	n/d	n/d	n/d	–	–
	Allantois	n/d	n/d	n/d	n/d	n/d	n/d	n/d	n/d	–	–
Staging	Initial host stage	EHF	vEHF	EHF	EHF	EHF	EHF	LHF	EHF	EHF	EHF
	Initial donor stage	EHF	EHF	EHF	EHF	EHF	EHF	EHF	EHF	EHF	EHF
	Final chimera stage	9–s	10–s	12–s	10–s	9–s	11–s	12–s	10–s	9–s	10–s

Gray highlight denotes statistically significant results ($p<0.05$).
+ denotes greater than 200 cells.
n/d denotes specimens not stained for STELLA.
[a]For immunostained specimens, includes STELLA-positive and -negative cells.
[b]Circulating within dorsal aortae, omphalomesenteric artery, and/or vessel of confluence.
[c]Includes general loose mesenchyme and/or mesoderm associated with somatopleure.

Table 5
Distribution of cells derived from distal ACD grafts in chimeras.

Tissue		Chimera number									
		1	2	3	4	5	6	7	8	9	10
Allantois (Total)[a]		+	+	+	+	+	+	+	+	+	+
Vessel endothelium	Dorsal aortae	–	–	–	–	–	–	–	–	–	5
	Omphalomesenteric artery	–	–	–	–	–	–	7	2	–	28
	Vessel of confluence	–	–	–	–	–	–	–	–	2	29
	Yolk sac	–	–	–	–	–	7	–	–	120	139
Hematopoietic cells	Posterior embryo[b]										8
	Yolk sac blood islands	–	–	–	–	–	–	–	–	2	8
Other tissues of the posterior embryo	Hindgut (Total)[a]	–	–	–	–	–	–	–	–	–	1
	Posterior mesoderm (Total)[a, c]	–	–	–	–	–	–	–	7	–	–
	Somatopleure	–	–	–	–	–	–	–	–	–	–
	Splanchnopleure	–	–	–	–	–	–	–	–	–	–
	Surface ectoderm (Total)[a]	–	–	–	–	–	–	–	–	–	–
	Ventral ectodermal ridge (Total)[a]	–	–	–	–	–	–	–	–	–	–
Other extraembryonic tissues	Yolk sac XVE	–	–	–	–	–	–	–	–	–	–
	Yolk sac mesothelium	–	–	–	–	–	–	–	–	3	–
	Amnion	–	–	–	–	–	–	–	–	–	–
STELLA-positive cells only	Hindgut	n/d	n/d	n/d	–	n/d	n/d	–	–	–	1
	Posterior mesoderm[c]	n/d	n/d	n/d	–	n/d	n/d	–	–	–	–
	Surface ectoderm	n/d	n/d	n/d	–	n/d	n/d	–	–	–	–
	Ventral ectodermal ridge	n/d	n/d	n/d	–	n/d	n/d	–	–	–	–
	Allantois	n/d	n/d	n/d	–	n/d	n/d	–	–	–	–
Staging	Initial host stage	EHF	EHF	LHF	EHF	EHF	EHF	EHF	LHF	LHF	LHF
	Initial donor stage	EHF	EHF	EHF	LHF	2-s	EHF	EHF	EHF	LHF	LHF
	Final chimera stage	11–s	12–s	12–s	12–s	12–s	9–s	11–s	11–s	9–s	11–s

Gray highlight denotes statistically significant results ($p<0.05$).
+ denotes greater than 200 cells.
n/d denotes specimens not stained for STELLA.
[a]For immunostained specimens, includes STELLA-positive and -negative cells.
[b]Circulating within dorsal aortae, omphalomesenteric artery, and/or vessel of confluence.
[c]Includes general loose mesenchyme and/or mesoderm associated with somatopleure.

On average, proximal ACD and distal ACD grafts contributed to a statistically greater length of the chimeric allantois than IPS or distal allantois grafts (Fig. 6). Although no differences in the length and distal-most site of contribution between grafts of proximal or distal ACD were observed ($p=0.2022$ and $p=0.3181$, respectively), proximal ACD grafts contributed to a more proximal region of the chimeric allantois than distal ACD grafts ($p=0.0040$; Fig. 6).

The IPS and distal allantois grafts contributed to statistically similar allantoic lengths ($p=0.1102$), but contribution from these two grafts varied based on their location within the length of the allantois (Fig. 6). The IPS graft contributed to the allantois's proximal-most region, while the distal allantois graft contributed to a more distal region of the allantois, to which the distal ACD graft also contributed (Fig. 6).

Discussion

In this study, we examined STELLA during a 54-hour time period, during which conceptuses were sampled at 2–4 hour intervals. Nuclear and cytoplasmic STELLA were found in multiple cell types both within and outside of the established PGC trajectory. Fate-mapping those posterior regions that contained nuclear STELLA at headfold-stages (~7.75–8.0 dpc) revealed that the proximal ACD and IPS, regions that contained the most abundant STELLA-positive cells, contributed to derivatives of all three primary germ layers. Colonization included STELLA-positive putative PGCs in the hindgut as well as STELLA-positive somatic cells in the ventral ectodermal ridge, posterior mesoderm, and allantois. Together, these results are consistent with the conclusion that regions containing nuclear STELLA contribute to a wider range of tissues than previously reported.

Admittedly, tissue fate-mapping is not equivalent to clonal lineage tracing. Ideally, clonal tracing a single STELLA-positive cell would reveal whether it ultimately ends up in the germ line. Unfortunately, no embryo culture method exists that will support development of labeled or grafted embryos outside of the uterus between 8.0 and 11.5 dpc, when putative PGCs translocate from their site of formation in the posterior region to the gonads. Thus, by taking an indirect approach to finding out whether STELLA-positive cells are found in tissues other than the hindgut, we have obtained data consistent with manifold and generalized roles of nuclear STELLA in cell populations emerging within the posterior region.

Advantages and validity of grafting large pieces of tissue over other grafting methods

The recently identified Allantoic Core Domain (ACD) encompasses approximately 120 μm of T-positive cells within the allantois (Downs et al., 2009), whose boundary with the embryo is traditionally defined as the site of insertion of the amnion into the epiblast. Prior to this study, the only known role of the ACD was as a cell reservoir that contributed abundantly to the allantois, thereby ensuring its elongation to the chorion (Downs et al., 2009). However, for technical reasons, only that part of the ACD above the allantoic site of insertion into the amnion and yolk sac had been fate-mapped (Downs and Harmann, 1997; Downs et al., 2009), as this is the part of the allantois that easily breaks off during the mouth aspiration procedure used to remove it for grafting (Fig. 1G). Others had fate-mapped the primitive streak just beneath the amniotic insertion (Beddington, 1982; Kinder et al., 1999; Tam and Beddington, 1987), but, to the best of our knowledge, no one has hitherto fate-mapped the headfold-stage small triangle of allantoic cells located between these two sites and which we found to be richly positive for STELLA (Fig. 1G).

Thus, in this study, we grafted the entire allantois, including the small triangle of tissue that was encompassed within the proximal

Table 6
Distribution of cells derived from proximal ACD grafts in chimeras.

Tissue		Chimera number																		
		1	2	3	4	5	6	7	8	9	10	11	12	13	14[a]	15	16	17	18	19
Allantois (Total)[b]		+	+	+	+	+	+	+	+	+	+	+	+	+	+	+	+	+	+	+
Vessel endothelium	Dorsal aortae	32	3	39	11	20	–	–	–	–	–	–	–	–	–	–	–	–	–	–
	Omphalomesenteric artery	26	8	8	96	33	99	15	19	–	16	2	5	–	–	–	–	–	–	–
	Vessel of confluence	28	3	11	31	8	–	–	–	3	2	–	–	–	–	–	–	–	–	–
	Yolk sac	8	–	–	9	–	5	15	–	–	–	8	–	51	–	–	–	–	–	–
Hematopoietic cells	Posterior embryo[c]	8	–	–	3	1	2	–	1	–	–	–	–	–	–	–	–	–	–	–
	Yolk sac blood islands	–	–	–	–	–	–	–	–	–	–	–	–	–	–	–	–	–	–	–
Other tissues of the posterior embryo	Hindgut (Total)[b]	41	15	14	5	19	6	4	4	33	–	–	–	–	–	–	–	–	–	–
	Posterior mesoderm (Total)[b, d]	136	9	17	23	16	–	17	3	9	5	–	–	–	–	–	–	–	–	–
	Somatopleure	–	–	–	–	–	–	–	–	–	–	–	–	–	–	–	–	–	–	–
	Splanchnopleure	17	10	13	3	–	–	–	–	–	–	10	10	–	–	–	–	–	–	–
	Surface ectoderm (Total)[b]	–	–	2	–	–	–	–	–	1	–	–	–	–	–	–	–	–	–	–
	Ventral ectodermal ridge (Total)[b]	–	–	–	–	–	–	–	–	–	–	–	–	–	–	–	–	–	–	–
Other extraembryonic tissues	Yolk sac XVE	–	–	–	–	–	–	–	–	–	–	–	–	–	–	–	–	–	–	–
	Yolk sac mesothelium	–	12	–	–	–	–	2	-	–	–	–	–	–	–	–	–	–	–	–
	Amnion	–	–	–	–	–	–	8	–	–	–	–	–	3	4	44	–	–	–	–
STELLA–positive cells only	Hindgut	n/d	6	3	2	9	n/d	n/d	n/d	n/d	n/d	n/d	n/d	n/d	n/d	n/d	n/d	–	–	–
	Posterior mesoderm[d]	n/d	1	–	–	–	n/d	n/d	n/d	n/d	n/d	n/d	n/d	n/d	n/d	n/d	n/d	–	–	–
	Surface ectoderm	n/d	–	1	–	–	n/d	n/d	n/d	n/d	n/d	n/d	n/d	n/d	n/d	n/d	n/d	–	–	–
	Ventral ectodermal ridge	n/d	–	–	–	–	n/d	n/d	n/d	n/d	n/d	n/d	n/d	n/d	n/d	n/d	n/d	–	–	–
	Allantois	n/d	5	18	28	–	n/d	n/d	n/d	n/d	n/d	n/d	n/d	n/d	n/d	n/d	n/d	–	27	1
Staging	Initial host stage	LHF	vEHF	LHF	EHF	EHF	2-s	EHF	LHF	LHF	EHF	EHF	EHF	vEHF	EHF	EHF	EHF	LHF	EHF	LHF
	Initial donor stage	EHF	vEHF	LHF	EHF	EHF	2–s	EHF	LHF	EHF	LHF	2–s	EHF	vEHF	EHF	EHF	EHF	EHF	EHF	LHF
	Final chimera stage	10–s	11–s	10–s	10–s	11–s	12–s	8–s	10–s	9–s	10–s	12–s	10–s	11–s	10–s	11–s	11–s	10–s	12–s	10–s

Gray highlight denotes statistically significant results ($p<0.05$).
+ denotes greater than 200 cells.
n/d denotes specimens not stained for STELLA.
[a]Chimera exhibited a host-derived double omphalomesenteric artery.
[b]For immunostained specimens, includes STELLA-positive and -negative cells.
[c]Circulating within dorsal aortae, omphalomesenteric artery, and/or vessel of confluence.
[d]Includes general loose mesenchyme and/or mesoderm associated with somatopleure.

ACD, as well as the underlying intraembryonic posterior primitive streak (IPS). Rather than use disaggregated clumps of 5–20 cells (Copp et al., 1986; Downs and Harmann, 1997; Kinder et al., 1999; Tam and Beddington, 1987), the tissue pieces used here contained approximately 100 cells. Thus, we avoided several technical pitfalls associated with the former technique. These included cell loss due to cell death and other technical considerations that may come from cell dissociation. In addition, because cell–cell contacts may be crucial to cell fate decisions within the posterior region, grafting cell clumps may potentially alter the fate of grafted cells by forcing cells to interact with cell types in the host with which they may not have interacted in the undisturbed donor conceptus, thereby skewing the fate map. Finally, fate-mapping analyses based on grafting cell clumps requires that graft contribution to a single cell type be compared to the total number of graft-derived cells within a set of chimeras. If contribution to a particular cell type is relatively small, it may be considered insignificant. By contrast, grafting pieces of tissue allows calculation of the frequency of contribution to compare and contrast adjacent regions, thereby permitting a larger snapshot of a given region at a given time. Therefore, contribution of small numbers of cells to a particular cell type may be considered significant if that contribution occurs at a high enough frequency, as is the case for proximal ACD-derived hematopoietic cells in this study (Table 6).

As our fate-mapping results of posterior region tissue at headfold stages generally accorded with previous results of orthotopically grafted cell clumps from the posterior streak and/or allantois at earlier neural plate stages (~7.0–7.5 dpc; Copp et al., 1986; Kinder et al., 1999; Tam and Beddington, 1987), and as each piece displayed distinct and consistent colonization profiles, we conclude that fate-mapping by grafting larger pieces of tissue is an experimentally valid technique. Furthermore, as numbers of host-derived STELLA-positive cells in the hindgut and other tissues of chimeras were similar to those of ex vivo and unoperated culture controls (Fig. 5I), the grafting procedure does not disrupt the deployment of the STELLA-positive population from the posterior region, thereby validating the use of grafting to fate-map tissues containing this population.

"Ectopic PGCs" may be part of a normal stem cell reservoir that encompasses the ACD

The ACD, whose properties suggest that it may be a stem cell reservoir, has only recently been identified (Downs et al., 2009). Prior to its discovery, the only stem cells thought to reside in the posterior region were PGCs. Any cells previously identified via putative PGC markers and found outside of the putative PGC trajectory, i.e., the base of the allantois, posterior embryonic/extraembryonic junction, hindgut, and gonads, were generally thought to be "ectopic PGCs" that will either become incorporated into their surrounding regions (Anderson et al., 2000) or apoptose without contributing to surrounding tissues (e.g., Tres et al., 2004). Although there is no evidence for the former possibility, embryos mutant for the pro-apoptotic gene *Bax* exhibited increased numbers of OCT-3/4-positive cells outside of the putative PGC trajectory during migration from the hindgut into the gonads at ~10.5 dpc, suggesting that at least some ectopic putative PGCs may normally apoptose (Stallock et al., 2003). However, the authors did not determine whether such "ectopic" putative PGCs contributed to surrounding tissues prior to apoptosis, nor did they examine earlier stages when the putative PGCs are migrating from the posterior embryonic–extraembryonic junction into the hindgut. Furthermore, although lineage-tracing studies have attempted to define the timepoint of lineage restriction of the putative PGCs in the embryonic–extraembryonic junction of the posterior

Table 7
Distribution of cells derived from IPS grafts in chimeras.

Tissue		Chimera number											
		1	2	3	4[a]	5	6	7	8	9	10	11	12[a]
Allantois (Total)[b]		+	+	+[4]	+	+	168	166	114	70	47	2	–
Vessel endothelium	Dorsal aortae	8	8	4	4	3	–	1	26	6	–	22	3
	Omphalomesenteric artery	–	–	17	–	4	–	6	18	–	–	–	10
	Vessel of confluence	5	17	8	22	14	74	7	46	–	–	–	4
	Yolk sac	2	–	–	–	9	–	–	–	–	–	–	–
Hematopoietic cells	Posterior embryo[d]	–	–	–	–	–	–	–	–	–	–	–	–
	Yolk sac blood islands	–	–	–	–	–	–	–	–	–	–	–	–
Other tissues of the posterior embryo	Hindgut (Total)[b]	20	3	5	–	48	–	8	4	–	8	138	10
	Posterior mesoderm (Total)[b, e]	+	+	+	+	119	+	+	+	+	+	+	+
	Somatopleure	171	146	112	+	21	30	+	+	141	177	+	100
	Splanchnopleure	+	+	+	+	53	+	+	+	147	196	+	+
	Surface ectoderm (Total)[b]	–	–	–	–	–	–	1	10	–	1	–	–
	Ventral ectodermal ridge (Total)[b]	–	–	–	–	–	26	–	39	–	–	–	–
Other extraembryonic tissues	Yolk sac XVE	8	–	–	–	–	–	–	–	–	–	–	–
	Yolk sac mesothelium	–	–	–	–	–	–	–	–	–	–	–	–
	Amnion	–	–	–	–	–	–	–	–	–	–	–	–
STELLA–positive cells only	Hindgut	1	1	5	–	2	–	1	–	–	4	3	2
	Posterior mesoderm[e]	3	15	3	–	–	–	14	–	–	–	–	–
	Surface ectoderm	–	–	–	–	–	–	1	–	–	–	–	–
	Ventral ectodermal ridge	–	–	–	–	–	12	–	7	–	–	–	–
	Allantois	1	–	7	–	1	–	–	–	–	–	–	–
Staging	Initial host stage	vEHF	EHF	EHF	EHF	EHF	LHF	EHF	LHF	LHF	EHF	LHF	LHF
	Initial donor stage	vEHF	EHF	EHF	EHF	EHF	LHF	EHF	LHF	EHF	EHF	LHF	LHF
	Final chimera stage	10–s	9–s	9–s	9–s	9–s	11–s	9–s	11–s	10–s	10–s	11–s	10–s

Gray highlight denotes statistically significant results ($p<0.05$).
+denotes greater than 200 cells.
[a]Chimera exhibited a host-derived double omphalomesenteric artery.
[b]For immunostained specimens, includes STELLA-positive and -negative cells.
[c]Circulating within dorsal aortae, omphalomesenteric artery, and/or vessel of confluence.
[d]Includes general loose mesenchyme and/or mesoderm associated with somatopleure.
[e]Includes contribution to ventral cuboidal mesothelium (VCM) of the allantois, observed 1 out of 12 times ($p=0.2678$); no contribution to dorsal cuboidal mesothelium (DCM) observed within this or any other chimera.

conceptus (Lawson and Hage, 1994; Ohinata et al., 2005), it remains unclear to what extent this "segregated" population subsequently contributes to the germ line and/or somatic populations.

Based on our results, we argue that "ectopic" PGCs may not be PGCs, but rather part of a larger posterior stem cell pool that includes the ACD. STELLA-positive cells localizing to the allantois and other tissues outside of the PGC trajectory were consistently observed in the same sites of multiple, if not all, same-stage specimens examined. Importantly, none of these STELLA-positive cells, either from cultured or uncultured specimens, appeared to be morphologically apoptotic. Similar results were found with other PGC "markers." For example, like STELLA, OCT-3/4 localized not only to the hindgut but also to the allantois and posterior surface ectoderm at 8–12-s (Anderson et al., 2000; Downs, 2008). Our results also accord with a previous fate-mapping study that reported the presence of graft-derived TNAP-positive cells not only in the hindgut, but also in the allantois and surface ectoderm (Copp et al., 1986), the latter of which, based on findings in the current study, may have been part of the ventral ectodermal ridge, which was not scored in those studies.

Intriguingly, graft-derived STELLA-positive cells outside of the hindgut, specifically in the allantois (Figs. 5C, G), posterior mesoderm (Figs. 5F), and ventral ectodermal ridge (Fig. 5E), were oftentimes closely associated with graft-derived STELLA-negative cells, suggesting that they may share a common precursor. A similar observation was reported for graft-derived TNAP-positive cells in the allantois and surface ectoderm (Copp et al., 1986). Whether some of these adjacent STELLA- or TNAP-negative cells are the daughters of STELLA- or TNAP-positive cells that underwent asymmetric division is an interesting question that remains to be explored.

Contribution of STELLA-positive cells from the proximal ACD and IPS to the posterior region, including putative PGCs in the hindgut, was unexpectedly small

At the time of grafting, headfold-stage proximal ACD and IPS contained an average of 41.6 and 31.1 STELLA-positive cells, respectively (Table 1). Yet after culture, proximal ACD and IPS grafts contributed relatively fewer total STELLA-positive cells to the posterior region (16.8 cells from the proximal ACD; 8.3 cells from the IPS; Table 8). As such cells are thought to be lineage-restricted PGCs (Ohinata et al., 2005; Saitou et al., 2002), one would have expected all of the STELLA-positive cells in the proximal ACD and IPS to contribute at least the same number of STELLA-positive cells to the hindgut. However, the proximal ACD and IPS grafts contributed even less to the hindgut (average of 5.0 and 2.4 cells, respectively, Table 8).

Several explanations for these unexpectedly low numbers are possible. First, although grafting large groups of cells was meant to circumvent the possibility of cell death, it is possible that many grafted STELLA-positive cells did not survive the microsurgery. Alternatively, separating the proximal ACD and IPS could have disrupted axial cues at the embryonic–extraembryonic junction that may have been required for maintaining the STELLA-positive population, leading to cell death. However, both scenarios are unlikely, as microsurgery at the posterior embryonic–extraembryonic junction did not affect the size of the host-derived STELLA-positive population in the hindgut and other tissues within operated chimeras compared to ex vivo specimens and unoperated controls (Fig. 5I).

Second, the number of STELLA-positive cells that colonize the hindgut might be tightly regulated, providing grafted STELLA-positive

Table 8
Average[a] contribution of graft-derived cells occurring at a statistically significant frequency in synchronous (approximate) orthotopic grafts.

Cell type		Distal allantois (sem)	Distal ACD (sem)	Proximal ACD (sem)	IPS (sem)
Allantois (Total)[b]		>200 (n/a)***	>200 (n/a)***	>200 (n/a)***	142.5 (21.9)[c];***
Vessel endothelium	Dorsal aortae	–	–	21.0 (6.6)***	8.5 (2.7)***
	Omphalomesenteric artery	34.0 (2.0)[d];*	12.3 (8.0)**	29.7 (10.5)***	11.0 (2.8)***
	Vessel of confluence	–	15.5 (13.5)*	12.3 (4.6)***	21.9 (7.8)***
	Yolk sac	65.7 (42.7)[d];**	88.7 (41.2)[d];**	16.0 (7.1)[d];***	5.5 (3.5)[d];*
Hematopoietic cells	Posterior embryo[e]	–	–	3.0 (1.3)***	–
	Yolk sac blood islands	–	5.0 (3.0)[d];*	–	–
Other tissues of the posterior embryo	Hindgut (Total)[b]	–	–	15.7 (4.5)***	27.1 (14.6)***
	Posterior mesoderm (Total)[b], [f]	–	–	26.1 (13.9)***	193.3 (6.8)[c];***
	Somatopleure	–	–	–	141.5 (18.5)[c];***
	Splanchnopleure	–	–	10.5 (1.9)***	183.0 (12.6)[c];***
	Surface ectoderm (Total)[b]	–	–	–	4.0 (3.0)**
	Ventral ectoderm ridge (total)[b]	–	–	–	32.5 (6.5)*
Other extraembryonic tissues	Yolk sac XVE	–	–	–	–
	Yolk sac mesothelium	–	–	–	–
	Amnion	–	–	14.8 (9.8)[d];**	–
STELLA-positive cells only	Hindgut	–	–	5.0 (1.6)***	2.4 (0.53)***
	Posterior mesoderm[f]	–	–	–	8.8 (3.3)***
	Surface ectoderm	–	–	–	–
	Ventral ectodermal ridge	–	–	–	9.5 (2.5)*
	Allantois	–	–	15.8 (5.5)***	3.0 (2.0)**
	Total	–	–	16.8 (4.61)***	8.3 (1.84)***

Statistical significance based on frequency of contribution, one-tailed exact binomial test.
Abbreviations: n/a, not applicable; sem, standard error of the mean; and xve, extraembryonic visceral endoderm.
[a] Average for each cell type calculated from only those chimeras exhibiting contribution to that cell type.
[b] For immunostained specimens, includes STELLA-positive and -negative cells.
[c] Underestimation of average graft contribution. See Materials and methods for details.
[d] Contribution may be an artifact of grafting technique and reflects graft potency but not fate; see Discussion.
[e] Circulating within dorsal aortae, omphalomesenteric artery, and/or vessel of confluence.
[f] Includes general loose mesenchyme and/or mesoderm associated with somatopleure.
*** $p<0.001$.
** $p<0.01$.
* $p<0.05$.

cells little opportunity to translocate to the hindgut. However, because the hindgut's STELLA-positive population exhibited great variability, ranging from 68 to 207 host-derived cells in chimeras with proximal ACD or IPS grafts, we feel that this possibility, too, is unlikely. Furthermore, this range is not unique to STELLA, as similarly large ranges in the size of the hindgut's putative PGC population were

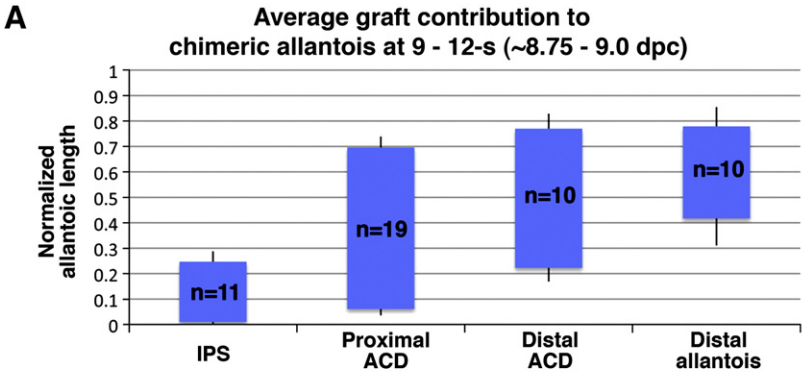

B

p-values for parameters of graft contribution

Parameter for comparison	Graft type	Graft type: Proximal ACD	Graft type: Distal ACD	Graft type: Distal allantois
Proximal-most graft contribution	IPS	p=0.1330	p=0.0006	p=0.0007
	Proximal ACD	-	p=0.0040	p=0.0002
	Distal ACD	-	-	p=0.1184
Distal-most graft contribution	IPS	p<0.0001	p<0.0001	p<0.0001
	Proximal ACD	-	p=0.3181	p=0.3095
	Distal ACD	-	-	p=0.9251
Length of graft contribution	IPS	p<0.0001	p<0.0001	p=0.1102
	Proximal ACD	-	p=0.2022	p=0.0010
	Distal ACD	-	-	p=0.0216

Fig. 6. Graft contribution along length of allantois at 9–12-s (~8.75–9.0 dpc). (A) Average graft contribution along normalized length of chimeric allantois, with 0 representing site of insertion into posterior embryo and 1 representing site of fusion with chorion. Error bars represent standard error of the mean (sem). (B) Analysis of proximal-most graft contribution, distal-most graft contribution, and total length of graft contribution via Student's *t*-test. Statistically significant differences ($p<0.05$) highlighted in blue.

observed by others using TNAP staining (Lawson et al., 1999; Ozdzenski, 1967).

The third possibility for limited graft contribution to STELLA-positive cells in the posterior region is that many STELLA-positive cells in the proximal ACD and IPS differentiate into STELLA-negative cells. This supports our hypothesis that STELLA-positive cells contribute to multiple cell types within the posterior region. Down-regulation of a more generalized stem cell pool could also explain the variability of STELLA-positive cells in the hindgut, discussed above. Experiments that employ transgenic strategies in which an endogenous expression mark persists even though cells have differentiated would be a critical tool to formally address the possibility that STELLA-positive cells give rise to STELLA-negative cells.

Finally, if the headfold-stage proximal ACD and IPS contribute only a small number of STELLA-positive cells to the hindgut, then the majority of the hindgut's STELLA-positive cells may be present in the headfold-stage AX and EVE (Fig. 1G), which contained STELLA but were not fate-mapped in our grafting experiments. Headfold-stage EVE is incorporated into the ventral hindgut (Franklin et al., 2008), and thus, the appearance of STELLA-positive nuclei within this tissue may represent the first wave of putative PGCs translocating into future hindgut endoderm. As we do not yet know whether headfold-stage AX is also incorporated into the hindgut, the significance of STELLA-positive cells localizing to this tissue remains unclear. However, results of previous studies have shown that the morphology of the AX becomes transformed from transitional cuboidal to squamous, typical of EVE, between neural plate and headfold stages (Downs et al., 2009; compare Figs. 1E–F to G). During this same period, the AX acquires OCT-3/4- (Downs, 2008) and T-positive nuclei (Downs et al., 2009) whose numbers fluctuate in tandem, suggesting that these cells may be used to build the posterior region under a yet-to-be-identified morphological clock (Downs et al., 2009). Here, we found STELLA-positive nuclei in the AX and EVE at similar stages (Fig. 1G). These STELLA-positive nuclei, which were absent from the AX and EVE during neural plate stages (Figs. 1E, F), may originate from the presumptive ACD and IPS. This accords with previous studies demonstrating the appearance of TNAP-positive cells in the endoderm overlying the posterior region at headfold stages (~7.75 dpc; Hara et al., 2009).

The endpoint of putative PGC translocation into (future) hindgut endoderm has yet to be defined. One study concluded that all TNAP-positive putative PGCs have completed translocation in hindgut endoderm by 3–4-s (~8.25 dpc; Hara et al., 2009) but at these same stages, we found that STELLA-positive cells persisted in the underlying ACD and IPS (Figs. 1A, I). Whether any of these remaining STELLA-positive cells translocate into the hindgut after 4-s is not known.

Intriguingly, the proximal ACD and IPS contributed more STELLA-negative than STELLA-positive cells to the ventral hindgut (Table 8). These proximal ACD and IPS-derived STELLA-negative cells could represent a wave of epiblast-derived cells that intercalate with and expand the EVE, part of which later forms the hindgut (Kwon et al., 2008). The mechanisms that initiate formation of the hindgut invagination remain obscure, but fate-mapping revealed that caudal-most EVE in the midline of the posterior headfold-stage embryo contributes primarily to ventral hindgut, rostral-most midline posterior EVE contributes primarily to dorsal hindgut, and midline posterior EVE between these two regions contributes to both ventral and dorsal hindgut (Franklin et al., 2008). Therefore, some cells from the IPS and proximal ACD may contribute to the caudal-most midline posterior EVE, thereby becoming incorporated into the ventral hindgut. At later stages (4–7-s), the posterior primitive streak continues to contribute endodermal cells that are incorporated into both the dorsal and ventral hindgut (Wilson and Beddington, 1996).

The ACD and IPS collaborate to build the posterior vasculature

Critical to the umbilical–fetal connection is the establishment of a unified circulatory system in which the embryonic dorsal aortae, yolk sac omphalomesenteric artery, and umbilical artery amalgamate, thereby uniting the three arterial vasculatures of the conceptus (Downs et al., 1998). Through establishment of the vessel of confluence, blood can be collected from the embryo and yolk sac at a single site before it is channeled into the placenta. However, because previous fate-mapping studies reported limited contribution to the posterior vasculature without distinguishing between the various vessels (Tam and Beddington, 1987), the origin of the posterior arterial vasculature remained obscure. Results from the present study demonstrated that distal ACD, proximal ACD, and IPS grafts all contribute to the vessel of confluence and omphalomesenteric artery (Table 5–8). In addition, the proximal ACD and IPS further contributed to the dorsal aortae (Table 6–8). These results indicate that the ACD and IPS cooperate to build the posterior vasculature.

The precise source of the vasculature within these regions is unknown. The rare formation of a double host-derived omphalomesenteric artery in some proximal ACD and IPS chimeras (Fig. 5H) suggests that the embryonic–extraembryonic junction contains dose-dependent signals responsible for regulating formation of the omphalomesenteric artery. Intriguingly, recent results from our laboratory have demonstrated the presence of abundant Hedgehog in this region (Daane and Downs, 2011), especially in the ventral cuboidal mesothelium (VCM), which was included in the grafted piece containing the distal ACD (Fig. 4A). While the VCM was impermeable to dextran challenge, it did not exhibit the properties of a typical epithelium, as tight junctions were absent (Daane et al., 2011). Given the presence of OCT-3/4- (Downs, 2008) and STELLA-positive cells (this study, Fig. 1J) in the VCM, it is tantalizing to speculate that the VCM may delaminate cells, possibly via Hedgehog signaling (reviewed in Kang and Svoboda, 2005) and contribute to the vessel of confluence.

The ACD, rather than the IPS, contains hematopoietic precursor cells

The allantois contains definitive hematopoietic potential (Corbel et al., 2007; Zeigler et al., 2006). RUNX1, required for hematopoietic stem cell formation (North et al., 2002), localizes to the allantois (Zeigler et al., 2006), and is found in both the nascent umbilical artery and vessel of confluence (Daane and Downs, 2011). However, whether the allantois contributes to the hematopoietic cell population in vivo remained obscure. In this study, the proximal ACD but not the IPS contributed a small number of circulating hematopoietic cells (Table 8). These hematopoietic cells were only observed in specimens with proximal ACD contribution to the posterior vasculature; therefore, results accord with reports demonstrating that blood cells bud off from hemangioblasts that line the arterial vasculature (Boisset et al., 2010; Chen et al., 2009). The small number of contributed hematopoietic cells may be the consequence of a first wave of hematopoietic cells budding off from proximal ACD-derived hemangioblasts. Perhaps allowing the chimeras to develop in culture for longer would produce more graft-derived hematopoietic cells. Alternatively, the observed contribution could represent a final wave of allantois-derived hematopoietic cells, suggesting that fate-mapping earlier-staged allantoises might provide greater hematopoietic contribution. Although the IPS did not contribute to hematopoietic cells in this study, it is possible that the primitive streak contributes to definitive hematopoiesis at stages prior to or after the headfold stages. Indeed, the IPS-derived ventral ectodermal ridge is not only STELLA-positive, but it also expresses *Runx1* (Daane and Downs, 2011), suggesting a role in hematopoiesis (Daane and Downs, 2011; Dyer et al., 2001; North et al., 2002).

Building the allantois is a collaborative process between the ACD and IPS

All four grafted subregions contributed to different segments of the chimeric allantois. However, approximately 70% of the allantois's length is built by the proximal and distal ACD, while the IPS and distal allantois

exhibited relatively minor contributions at the headfold stage (Fig. 6). These results accord with previous reports which concluded that the ACD is responsible for allantoic elongation (Downs et al., 2009) and that the allantois is regionalized by the headfold stage (Downs and Harmann, 1997).

However, in the present study, the analysis of graft contribution along the length of the allantois failed to account for the origin of the distal-most 15% of the allantois (Fig. 6A). This might be an experimental artifact from approximate orthotopic grafting the distal ACD and distal allantois into the host's proximal ACD, rather than directly into their homologous sites, which is technically more difficult. Although the grafted distal ACD and distal allantois were distinguishable from the proximal ACD in their contribution to the chimeric allantois (Fig. 6), it is possible that they would have displayed more distal contribution along the length of the allantois had they been grafted precisely into the host's distal ACD or distal allantois. Nevertheless, despite being grafted into the proximal region of the allantois, the majority of distal allantoic grafts ended up in the distal region, providing further evidence for regionalization of allantoic subregions at the headfold stage (Downs and Harmann, 1997; Downs et al., 1998).

Unexpectedly, all graft types contributed to yolk sac endothelium (Tables 4–8). In addition, the distal allantois contributed to the omphalomesenteric artery (Tables 4, 8), and the distal ACD contributed to hematopoietic cells in the yolk sac (Tables 5, 8). In all cases, this contribution may reflect tissue potential rather than fate for several reasons. First, previous studies revealed that allantoic cells generally translocate from proximal-to-distal (Downs and Harmann, 1997; Downs et al., 2009). Thus, distal allantois and distal ACD grafts were expected to contribute exclusively to more distal regions of the chimeric allantois while the proximal ACD and IPS were expected to contribute to tissues at the embryonic–extraembryonic junction. Second, previous fate-mapping experiments of cell clumps derived from the distal allantois and distal ACD did not demonstrate contribution outside of the allantois (Downs and Harmann, 1997). Third, when ectopically integrated into a damaged yolk sac, allantoises contributed both endothelial and hematopoietic cells at the site of damage, thereby indicating the allantois's potential to contribute to yolk sac lineages (Downs et al., 1998).

Intriguingly, while the proximal ACD also contributed to the amnion (Tables 6, 8), it is not clear whether the contribution represents true fate or potency. This is because amniotic contribution did not occur in that amnion adjacent to the dorsal cuboidal mesothelium (DCM), which may play a role in amnion formation (Daane and Downs, 2011) and which was included in proximal ACD grafts (Fig. 4A). Instead, this contribution occurred in amniotic tissue some distance from the DCM, but which was physically apposed to graft-derived distal allantoic tissue. Under normal circumstances, the amnion enlarges and becomes closely associated with the allantois (Daane et al., 2011; Downs et al., 2002). Whether these two tissues normally exchange and/or replace each other's cells is not known. Nevertheless, this apposition and allantoic graft contribution to the amnion highlights the close interaction between the elongated allantois and the expanding amnion. Alternatively, we cannot rule out the possibility that this pattern of contribution is an artifact of grafting that resulted from amnion that was inadvertently damaged during microsurgery.

The IPS contributes to the proximal umbilical cord and posterior embryonic ventral surface

Results of previous limited fate-mapping studies by DiI labeling and grafting suggested that the proximal midline of the allantois is established by the ACD, while the IPS contributes to the proximal allantoic flanks (Downs et al., 2009). Here, although we found contribution from the IPS to the proximal allantoic core, we did not identify IPS contribution to the ventral and dorsal cuboidal mesothelia (VCM and DCM; Table 7), which are distinct proximal walls of the allantois that appear by the headfold stage (Daane et al., 2011). These observations suggest that the VCM and DCM might be established at an earlier stage. By contrast, the IPS exhibited significant contribution to the posterior embryo's somatopleure and splanchnopleure, which cover the lateral and mid-ventral surfaces, respectively, prior to formation of the definitive body wall. The somatopleure and splanchnopleure are derived from lateral plate mesoderm (Funayama et al., 1999), which in turn is derived, in part, from the posterior primitive streak (equivalent to the IPS in this study; Tam and Beddington, 1987). Therefore, results from this study indicate that such mesoderm that leaves the IPS at headfold stages is destined, in part, to contribute to the somatopleure and splanchnopleure.

There is some speculation that the splanchnopleure and somatopleure together form a primary ventral body wall, which may ultimately be replaced at 12.0 dpc by the definitive body wall (Brewer and Williams, 2004). Defects in body wall closure are often associated with defects in the umbilical cord, yet a unifying developmental program between the allantois and fetus remains obscure. It is tantalizing to speculate that, based on our fate-mapping results, umbilical-fetal defects could originate as early as ~7.75–8.0 dpc within the ACD/IPS.

Molecular control of differentiation in the posterior niche

If the STELLA-positive population of the posterior region is part of a larger, more generalized stem cell pool, then what are the molecular components involved in channeling and/or promoting differentiation of these putative stem cells into different lineages? The pathways of BMP4, BMP8b, and SMAD5 may be involved, as embryos lacking these molecules contained “ectopic PGCs,” identified via TNAP activity and/or OCT-3/4, within the amnion and/or allantois (Chang and Matzuk, 2001; Fujiwara et al., 2001; Ying et al., 2000). Therefore, if the putative PGCs are part of a larger posterior niche that contributes to the posterior region of the conceptus, then previously reported ectopic localization of the putative PGCs in such scenarios may need re-interpretation. For example, because a small number of STELLA-positive cells was observed in the amnion and allantois of wildtype conceptuses (Figs. 1F, G, I), the “ectopic PGCs” reported in mutants might be the result of a greater number of putative PGCs being directed into somatic lineages than occurs in wildtype conceptuses. Alternatively, these “ectopic PGCs” could, in fact, be cells that are normally channeled into the allantois and amnion but which are exhibiting delayed down-regulation of putative PGC markers that would otherwise occur in wildtype settings. Intriguingly, mutants for BMP4, BMP8b, and SMAD5 also exhibit defects in allantoic elongation (reviewed in Inman and Downs, 2007); the association between PGC defects and defects in allantoic elongation suggests that the putative PGCs are part of a larger stem cell pool, which includes the ACD, required for both proper formation and/or deployment of the putative PGC population and allantois.

Significance of non-nuclear STELLA

Non-nuclear STELLA was observed in vesicles of some cells of the yolk sac blood islands, and diffuse STELLA was seen in chorionic ectoderm. STELLA, which contains a putative nuclear localization signal and nuclear export signal, can be shuttled back and forth between the nucleus and cytoplasm (Nakamura et al., 2007; Saitou et al., 2002). Therefore, STELLA's known function as a protector against DNA demethylation may be regulated by the protein's subcellular localization. Intriguingly, STELLA in the chorionic ectoderm was observed at stages when trophoblast stem cells are present in this tissue (Uy et al., 2002).

Conclusions

By subdividing the T-defined ACD into distal and proximal components, we have demonstrated that the ACD contributes not only to the allantois, but to the embryo as well, including the hindgut,

splanchnopleure, posterior vasculature, and hematopoietic cells. These results support the notion that the primitive streak extends its reach into the extraembryonic region where it continues to undergo an epithelial-to-mesenchymal transition, creating mesoderm that contributes to both the allantois and fetus.

Based on STELLA localization in histological sections and fate-mapping of the ACD and surrounding posterior region in conjunction with STELLA immunostaining, we have further provided new insight into the population dynamics of the posterior region's STELLA-positive cells at the headfold stage, indicating that only a fraction of this population ultimately translocates into the hindgut endoderm as putative PGCs. These population dynamics were not reflected in the results of previous studies examining the timing of lineage restriction of the putative PGCs because those studies ended within the base of the allantois and prior to putative PGC entry into the hindgut (Lawson and Hage, 1994; Ohinata et al., 2005). When those studies were carried out, the existence of the ACD was not known. Therefore, by placing results from the present study within the context of the identity and properties of the ACD, we propose that STELLA identifies a broader pool of cells than previously recognized, which contributes to both the germ line and derivatives of all three primary germ layers within the posterior conceptus. However, further experiments are needed to trace the fate of individual STELLA-positive cells in the posterior region of the conceptus.

Acknowledgments

The authors thank Dr. Tara Becker (Department of Biostatistics and Medical Informatics) for her assistance with the statistics. This study was supported by grants from the March of Dimes (1-FY09-511) and National Institutes of Child Health and Development (R01 HD042706) (K.M.D.). M.M.M. is a National Science Foundation Graduate Research Fellow and was further supported by a pre-doctoral fellowship from the Stem Cell and Regenerative Medicine Center at the University of Wisconsin-Madison School of Medicine and Public Health.

References

Anderson, R., Copeland, T.K., Scholer, H., Heasman, J., Wylie, C., 2000. The onset of germ cell migration in the mouse embryo. Mech. Dev. 91, 61–68.
Beddington, R.S.P., 1982. An autoradiographic analysis of tissue potency in different regions of the embryonic ectoderm during gastrulation in the mouse. J. Embryol. Exp. Morphol. 69, 265–285.
Beddington, R.S.P., 1987. Isolation, culture and manipulation of post-implantation mouse embryos. In: Monk, M. (Ed.), Mammalian Development: A Practical Approach. IRL Press, Oxford, pp. 43–69.
Boisset, J.C., van Cappellen, W., Andrieu-Soler, C., Galjart, N., Dzierzak, E., Robin, C., 2010. In vivo imaging of haematopoietic cells emerging from the mouse aortic endothelium. Nature 464, 116–120.
Bortvin, A., Goodheart, M., Liao, M., Page, D.C., 2004. Dpp a3/Pgc7/stella is a maternal factor and is not required for germ cell specification in mice. BMC Dev. Biol. 4, 2.
Bowles, J., Teasdale, R.P., James, K., Koopman, P., 2003. Dpp a3 is a marker of pluripotency and has a human homologue that is expressed in germ cell tumours. Cytogenet. Genome Res. 101, 261–265.
Brewer, S., Williams, T., 2004. Finally, a sense of closure? Animal models of human ventral body wall defects. Bioessays 26, 1307–1321.
Chang, H., Matzuk, M.M., 2001. Smad5 is required for mouse primordial germ cell development. Mech. Dev. 104, 61–67.
Chen, M.J., Yokomizo, T., Zeigler, B.M., Dzierzak, E., Speck, N.A., 2009. Runx1 is required for the endothelial to haematopoietic cell transition but not thereafter. Nature 457, 887–891.
Chiquoine, A.D., 1954. The identification, origin, and migration of the primordial germ cells in the mouse embryo. Anat. Rec. 118, 135–146.
Copp, A.J., Roberts, H.M., Polani, P.E., 1986. Chimerism of primordial germ cells in the early postimplantation mouse embryo following microsurgical grafting of posterior primitive streak cells in vitro. J. Embryol. Exp. Morphol. 95, 95–115.
Corbel, C., Salaun, J., Belo-Diabangouaya, P., Dieterlen-Lievre, F., 2007. Hematopoietic potential of the pre-fusion allantois. Dev. Biol. 301, 478–488.
Daane, J.M., Downs, K.M., 2011. Hedgehog signaling in the posterior region of the mouse gastrula suggests manifold roles in the fetal-umbilical connection and posterior morphogenesis. Developmental Dynamics 240, 2175–2193.
Daane, J.M., Enders, A.C., Downs, K.M., 2011. Mesothelium of the murine allantois exhibits distinct regional properties. J. Morphol. 272, 536–556.
Downs, K.M., 2006. In vitro methods for studying vascularization of the murine allantois and allantoic union with the chorion. Methods Mol. Med. 121, 241–272.
Downs, K.M., 2008. Systematic localization of Oct-3/4 to the gastrulating mouse conceptus suggests manifold roles in mammalian development. Dev. Dyn. 237, 464–475.
Downs, K.M., Davies, T., 1993. Staging of gastrulating mouse embryos by morphological landmarks in the dissecting microscope. Development 118, 1255–1266.
Downs, K.M., Harmann, C., 1997. Developmental potency of the murine allantois. Development 124, 2769–2780.
Downs, K.M., Gifford, S., Blahnik, M., Gardner, R.L., 1998. Vascularization in the murine allantois occurs by vasculogenesis without accompanying erythropoiesis. Development 125, 4507–4520.
Downs, K.M., McHugh, J., Copp, A.J., Shtivelman, E., 2002. Multiple developmental roles of Ahnak are suggested by localization to sites of placentation and neural plate fusion in the mouse conceptus. Mech. Dev. 119, S31–S38.
Downs, K.M., Inman, K.E., Jin, D.X., Enders, A.C., 2009. The Allantoic Core Domain: new insights into the development of the murine allantois and its relation to the primitive streak. Dev. Dyn. 238, 532–553.
Dyer, M.A., Farrington, S.M., Mohn, D., Munday, J.R., Baron, M.H., 2001. Indian hedgehog activates hematopoiesis and vasculogenesis and can respecify prospective neurectodermal cell fate in the mouse embryo. Development 128, 1717–1730.
Franklin, V., Khoo, P.L., Bildsoe, H., Wong, N., Lewis, S., Tam, P.P.L., 2008. Regionalisation of the endoderm progenitors and morphogenesis of the gut portals of the mouse embryo. Mech. Dev. 125, 587–600.
Friedrich, G., Soriano, P., 1991. Promoter traps in embryonic stem cells: a genetic screen to identify and mutate developmental genes in mice. Genes Dev. 5, 1513–1523.
Fujiwara, T., Dunn, N.R., Hogan, B.L.M., 2001. Bone morphogenetic protein 4 in the extraembryonic mesoderm is required for allantois development and the localization and survival of primordial germ cells in the mouse. Proc. Natl. Acad. Sci. U. S. A. 98, 13739–13744.
Funayama, N., Sato, Y., Matsumoto, K., Ogura, T., Takahashi, Y., 1999. Coelom formation: binary decision of the lateral plate mesoderm is controlled by the ectoderm. Development 126, 4129–4138.
Ginsburg, M., Snow, M.H.L., McLaren, A., 1990. Primordial germ cells in the mouse embryo during gastrulation. Development 110, 521–528.
Goldman, D.C., Martin, G.R., Tam, P.P.L., 2000. Fate and function of the ventral ectodermal ridge during mouse tail development. Development 127, 2113–2123.
Grüneberg, H., 1956. A ventral ectodermal ridge of the tail in mouse embryos. Nature 177, 787–788.
Hara, K., Kanai-Azuma, M., Uemura, M., Shitara, H., Taya, C., Yonekawa, H., Kawakami, H., Tsunekawa, N., Kurohmaru, M., Kanai, Y., 2009. Evidence for crucial role of hindgut expansion in directing proper migration of primordial germ cells in mouse early embryogenesis. Dev. Biol. 330, 427–439.
Inman, K.E., Downs, K.M., 2007. The murine allantois: emerging paradigms in development of the mammalian umbilical cord and its relation to the fetus. Genesis 45, 237–258.
Kang, P., Svoboda, K.K.H., 2005. Epithelial–mesenchymal transformation during craniofacial development. J. Dent. Res. 84, 678–690.
Kinder, S.J., Tsang, T.E., Quinlan, G.A., Hadjantonakis, A.K., Nagy, A., Tam, P.P.L., 1999. The orderly allocation of mesodermal cells to the extraembryonic structures and the anteroposterior axis during gastrulation of the mouse embryo. Development 126, 4691–4701.
Kruegel, J., Miosge, N., 2010. Basement membrane components are key players in specialized extracellular matrices. Cell. Mol. Life Sci. 67, 2879–2895.
Kurimoto, K., Yabuta, Y., Ohinata, Y., Shigeta, M., Yamanaka, K., Saitou, M., 2008. Complex genome-wide transcription dynamics orchestrated by Blimp1 for the specification of the germ cell lineage in mice. Genes Dev. 22, 1617–1635.
Kwon, G.S., Viotti, M., Hadjantonakis, A.K., 2008. The endoderm of the mouse embryo arises by dynamic widespread intercalation of embryonic and extraembryonic lineages. Dev. Cell 15, 509–520.
Lawson, K.A., Hage, W.J., 1994. Clonal analysis of the origin of primordial germ cells in the mouse. In: Chadwick, D.J., Marsh, J. (Eds.), Germline Development. Wiley, Chichester, pp. 68–84.
Lawson, K.A., Dunn, N.R., Roelen, B.A.J., Zeinstra, L.M., Davis, A.M., Wright, C.V.E., Korving, J., Hogan, B.L.M., 1999. Bmp4 is required for the generation of primordial germ cells in the mouse embryo. Genes Dev. 13, 424–436.
Macgregor, G.R., Zambrowicz, B.P., Soriano, P., 1995. Tissue nonspecific alkaline phosphatase is expressed in both embryonic and extraembryonic lineages during mouse embryogenesis but is not required for migration of primordial germ cells. Development 121, 1487–1496.
Marthiens, V., Kazanis, I., Moss, L., Long, K., ffrench-Constant, C., 2010. Adhesion molecules in the stem cell niche — more than just staying in shape? J. Cell Sci. 123, 1613–1622.
McCoshen, J.A., McCallion, D.J., 1975. Study of primordial germ cells during their migratory phase in Steel mutant mice. Experientia 31, 589–590.
Mikedis, M.M., Downs, K.M., 2009. Collagen type IV and Perlecan exhibit dynamic localization in the Allantoic Core Domain, a putative stem cell niche in the murine allantois. Dev. Dyn. 238, 3193–3204.
Mintz, B., 1957. Embryological development of primordial germ-cells in the mouse: influence of a new mutation. J. Embryol. Exp. Morphol. 5, 396–403.
Mintz, B., Russell, E.S., 1957. Gene-induced embryological modifications of primordial germ cells in the mouse. J. Exp. Zool. 134, 207–237.
Molyneaux, K., Wylie, C., 2004. Primordial germ cell migration. Int. J. Dev. Biol. 48, 537–544.
Nakamura, T., Arai, Y., Umehara, H., Masuhara, M., Kimura, T., Taniguchi, H., Sekimoto, T., Ikawa, M., Yoneda, Y., Okabe, M., Tanaka, S., Shiota, K., Nakano, T., 2007. PGC7/Stella protects against DNA demethylation in early embryogenesis. Nat. Cell Biol. 9, 64–U81.
North, T.E., de Bruijin, M., Stacy, T., Talebian, L., Lind, E., Robin, C., Binder, M., Dzierzak, E., Speck, N.A., 2002. Runx1 expression marks long-term repopulating hematopoietic stem cells in the midgestation mouse embryo. Immunity 16, 661–672.

Ohinata, Y., Payer, B., O'Carroll, D., Ancelin, K., Ono, Y., Sano, M., Barton, S.C., Obukhanych, T., Nussenzweig, M., Tarakhovsky, A., Saitou, M., Surani, M.A., 2005. Blimp1 is a critical determinant of the germ cell lineage in mice. Nature 436, 207–213.

Ohta, S., Suzuki, K., Tachibana, K., Tanaka, H., Yamada, G., 2007. Cessation of gastrulation is mediated by suppression of epithelial–mesenchymal transition at the ventral ectodermal ridge. Development 134, 4315–4324.

Ozdzenski, W., 1967. Observations on the origin of primordial germ cells in the mouse. Zool. Pol. 17, 367–381.

Payer, B., Saitou, M., Barton, S.C., Thresher, R., Dixon, J.P.C., Zahn, D., Colledge, W.H., Carlton, M.B.L., Nakano, T., Surani, M.A., 2003. stella is a maternal effect gene required for normal early development in mice. Curr. Biol. 13, 2110–2117.

Payer, B., Lopes, S., Barton, S.C., Lee, C., Saitou, M., Surani, M.A., 2006. Generation of stella-GFP transgenic mice: a novel tool to study germ cell development. Genesis 44, 75–83.

Saitou, M., Barton, S.C., Surani, M.A., 2002. A molecular programme for the specification of germ cell fate in mice. Nature 418, 293–300.

Sato, M., Kimura, T.U., Kurokawa, K., Fujita, Y., Abe, K., Masuhara, M., Yasunaga, T., Ryo, A., Yamamoto, M., Nakano, T., 2002. Identification of PGC7, a new gene expressed specifically in preimplantation embryos and germ cells. Mech. Dev. 113, 91–94.

Scholer, H.R., Dressler, G.R., Balling, R., Rohdewohld, H., Gruss, P., 1990. Oct-4 — a germline specific transcription factor mapping to the mouse T-complex. EMBO J. 9, 2185–2195.

Seki, Y., Yamaji, M., Yabuta, Y., Sano, M., Shigeta, M., Matsui, Y., Saga, Y., Tachibana, M., Shinkai, Y., Saitou, M., 2007. Cellular dynamics associated with the genome-wide epigenetic reprogramming in migrating primordial germ cells in mice. Development 134, 2627–2638.

Stallock, J., Molyneaux, K., Schaible, K., Knudson, C.M., Wylie, C., 2003. The pro-apoptotic gene Bax is required for the death of ectopic primordial germ cells during their migration in the mouse embryo. Development 130, 6589–6597.

Tam, P.P.L., Beddington, R.S.P., 1987. The formation of mesodermal tissues in the mouse embryo during gastrulation and early organogenesis. Development 99, 109–126.

Tam, P.P.L., Snow, M.H.L., 1981. Proliferation and migration of primordial germ cells during compensatory growth in mouse embryos. J. Embryol. Exp. Morphol. 64, 133–147.

Tam, P.P.L., Tan, S.S., 1992. The somitogenetic potential of cells in the primitive streak and the tail bud of the organogenesis-stage mouse embryo. Development 115, 703–715.

Tres, L.L., Rosselot, C., Kierszenbaum, A.L., 2004. Primordial germ cells: what does it take to be alive? Mol. Reprod. Dev. 68, 1–4.

Uy, G.D., Downs, K.M., Gardner, R.L., 2002. Inhibition of trophoblast stem cell potential in chorionic ectoderm coincides with occlusion of the ectoplacental cavity in the mouse. Development 129, 3913–3924.

Vincent, S.D., Dunn, N.R., Sciammas, R., Shapiro-Shalef, M., Davis, M.M., Calame, K., Bikoff, E.K., Robertson, E.J., 2005. The zinc finger transcriptional repressor Blimp1/Prdm1 is dispensable for early axis formation but is required for specification of primordial germ cells in the mouse. Development 132, 1315–1325.

Wilson, V., Beddington, R.S.P., 1996. Cell fate and morphogenetic movement in the late mouse primitive streak. Mech. Dev. 55, 79–89.

Ying, Y., Liu, X.M., Marble, A., Lawson, K.A., Zhao, G.Q., 2000. Requirement of Bmp8b for the generation of primordial germ cells in the mouse. Mol. Endocrinol. 14, 1053–1063.

Zeigler, B.M., Sugiyama, D., Chen, M., Guo, Y.L., Downs, K.M., Speck, N.A., 2006. The allantois and chorion, when isolated before circulation or chorio-allantoic fusion, have hematopoietic potential. Development 133, 4183–4192.